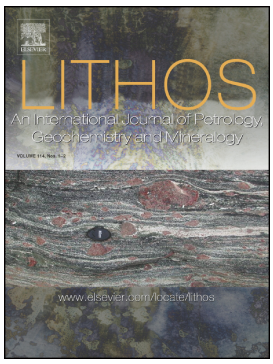

Chromitite petrogenesis in the mantle section of the Ballantrae Ophiolite complex (Scotland)

E.J. Derbyshire, B. O'Driscoll, D. Lenaz, A. Zanetti, R. Gertisser

PII: S0024-4937(19)30253-1
DOI: https://doi.org/10.1016/j.lithos.2019.06.013
Reference: LITHOS 5111

To appear in: *LITHOS*

Received date: 27 February 2019
Accepted date: 12 June 2019" role="suppressed

Please cite this article as: E.J. Derbyshire, B. O'Driscoll, D. Lenaz, et al., Chromitite petrogenesis in the mantle section of the Ballantrae Ophiolite complex (Scotland), LITHOS, https://doi.org/10.1016/j.lithos.2019.06.013

Chromitite petrogenesis in the mantle section of the Ballantrae Ophiolite Complex (Scotland)

Derbyshire, EJ[1], O'Driscoll, B[2,*] brian.odriscoll@manchester.ac.uk, Lenaz, D[3], Zanetti, A[4] and Gertisser, R[1]

[1]School of Geography, Geology and the Environment, Keele University, Keele, ST5 5BG, UK
[2]School of Earth and Environmental Sciences, University of Manchester, Oxford Road, M13 9PL, UK
[3]Dipartimento di Matematica e Geoscienze, Università degli Studi di Trieste, Trieste, I-34127, Italy
[4]Istituto di Geoscienze e Georisorse, C.N.R., Pavia, Italy
[*]Corresponding author.

For submission to: **Lithos**

Abstract

Podiform chromitites from the Ballantrae Ophiolite Complex (BOC), NW Scotland, are examined to investigate their petrogenesis and elucidate the nature of melt percolation in the supra-subduction zone oceanic mantle more generally. The mantle portion of the BOC comprises two petrologically distinct serpentinite belts, whose differences have previously been attributed to different degrees of upper mantle melt extraction. Chromitite occurs in each of the northern and southern serpentinite belts, at Pinbain Bridge and Poundland Burn, respectively. Field relationships suggest that chromitites were formed by melt-rock reaction in channel-like conduits in the upper mantle. Chromitite Cr-spinel compositions from the two localities show marked differences to one another, with the Pinbain Bridge chromitite Cr-spinels being characterised by relatively high Cr# [Cr/(Cr+Al); 0.62-0.65] and lower abundances of certain trace elements (e.g., Ti, Ga, V), whereas the Poundland Burn chromitite Cr-spinels exhibit relatively low Cr# (0.44-0.46) and higher concentrations of these trace elements. The contrasting Cr-spinel compositions are used to estimate parental magma compositions for the chromitites; the Pinbain Bridge chromitites crystallised from magmas resembling arc tholeiites whereas MORB-like magmas were involved in formation of the Poundland Burn chromitites. While it is possible that this dichotomy points to early derivation of the BOC at a MORB spreading centre, with subsequent processing in a supra-subduction zone, we suggest that the differences reflect melt extraction from different parts of an evolving subduction zone, such that the MORB-like magmas were generated in a back-arc setting. This interpretation

finds support in the Ti/Fe^3# versus Ga/Fe^3# systematics of peridotite-hosted accessory Cr-spinel that we present here, as well as previously published trace element data and geochronological constraints on the basalt lava sequences associated with the BOC, which collectively favour formation of the Poundland Burn chromitites in supra-subduction zone mantle.

Keywords: Ballantrae Ophiolite Complex, supra-subduction zone, podiform chromitite, upper mantle melt percolation

1. Introduction

The harzburgitic mantle sections of some supra-subduction ophiolites preserve a rich petrological and geochemical record of melt percolation and melt-rock reaction (e.g., Boudier and Nicolas, 1995; Bédard and Hébert, 1998; Piccardo et al. 2007; Rampone et al. 2008; Batanova et al., 2011; Derbyshire et al. 2013; O'Driscoll et al., 2015). The harzburgite typically hosts veins and sheets of dunite, pyroxenite and chromitite (>60 vol.% Cr-spinel) that point to a predominance of channelized, rather than porous, melt percolation in the mantle wedge (e.g., Maaløe, 2005; Batanova et al., 2011). Considerable complexity has been documented in the field relations and other characteristics of these 'fossil' upper mantle melt conduit systems, leading to interpretations invoking multiple generations of melt extraction. For example, O'Driscoll et al. (2015) employed Os isotopes and highly siderophile element abundances to argue that chromitites and orthopyroxenites in the ~497 Ma Leka Ophiolite Complex (Norway) formed during subduction-related melt percolation as the Iapetus Ocean closed, but that the websterites there may have formed ~80 Ma earlier, during Iapetus opening. Compositional variation in Cr-spinel in mantle peridotites and chromitites has also been utilised to elucidate a range of conditions of partial melting and melt percolation in the oceanic mantle, even within the same ophiolite. Cr-spinel is relatively resistant to low temperature alteration during the serpentinisation of mantle peridotites, facilitating its use as a petrogenetic fingerprinting tool. In a study that showed how Cr-spinel chemistry could be used to

decipher multiple melt extraction events, Melcher et al. (1997) reported two populations of chromitites in the Kempirsai ophiolite (Kazakhstan), one with high Cr# [Cr/(Cr+Al)] Cr-spinel and one with relatively low Cr# Cr-spinel. The low Cr# chromitites were attributed to low degree partial melting and melt percolation beneath an oceanic spreading centre (i.e., mid-ocean ridge; MOR), whilst the high Cr# chromitites were attributed to the comparatively high degrees of partial melting and fluxing of hydrous melts through a mantle wedge above a subduction zone (supra-subduction zone; SSZ). Thus, the mantle portion of the Kempirsai ophiolite was suggested to preserve evidence of ocean opening and closing, over a period of ≥50 My.

An increasing number of studies in recent years have recognised that podiform chromitites form by processes of melt percolation and consequent melt-rock reaction in the upper mantle (see Arai and Miura 2016 for a review). Podiform chromitites that preserve a bimodal distribution of Cr# compositions have been recorded in the mantle sections of other ophiolites, including the Semail Ophiolite (Oman; Ahmed and Arai, 2002; Rollinson, 2008), the Mayarí-Cristal Ophiolite (Cuba; González-Jiménez *et al.*, 2011), the Muğla Ophiolite (Turkey; Uysal et al., 2009) and the Luobusa Ophiolite (Tibet; Zhou *et al.*, 1996). Zhou and Robinson (1997), Ahmed and Arai (2002), Uysal et al. (2009) and Xiong et al. (2017) all invoke a model similar to that proposed by Melcher et al. (1997), whereby relatively low degrees of (anhydrous) partial melting at a MOR was followed by higher degrees of (hydrous) partial melting of an already depleted mantle source in a SSZ setting, forming Al- and Cr-rich chromitites, respectively. However, an alternative model proposes chromitite Cr-spinel compositions are temporally controlled by the progressive release of fluids, water and/or melt from the subducting slab during subduction zone development and progressive mantle depletion, forming increasingly Cr-rich chromitites over time (Zhou *et al.*, 1996; Arai, 1997; Büchl *et al.*, 2004; Rollinson, 2008; González-Jiménez *et al.*, 2011; Whattam and Stern, 2011).

The Ballantrae Ophiolite Complex (BOC; Scotland) is a potentially useful locality to examine the extent to which the supra-subduction mantle wedge records evidence of multiple episodes of melt percolation. Firstly, geochemical studies of the lava sequences and poorly-exposed

sheeted dykes have revealed broad spectrums of REE trends, ranging from LREE-enriched to LREE-depleted patterns (e.g., Wilkinson and Cann, 1974; Jones, 1977; Lewis and Bloxam, 1977; Thirlwall and Bluck, 1984; Smellie and Stone, 1992, 2001; Smellie *et al.*, 1995; Oliver and McAlpine, 1998). This led to extensive debate about the tectonic provenance of the BOC; proposed settings involve melt generation in an island arc with a back-arc basin, a MOR, a volcanic arc and the involvement of a mantle plume in the formation of the ophiolite (Wilkinson and Cann, 1974; Jones, 1977; Lewis and Bloxam, 1977; Thirlwall and Bluck, 1984; Oliver and McAlpine, 1998; Smellie and Stone, 2001). In addition, it has been suggested that the mantle portion of the BOC has been processed in different tectonic settings (Stone, 2014). In particular, the two broad serpentinite belts that comprise the BOC mantle have different petrological characteristics and sparse data published on the podiform chromitites hosted in each suggests significant differences in chromitite Cr-spinel Cr# exist (**Fig. 1**; Stone and Smellie, 1988; Stone, 2014). In this study, we present detailed new petrological and mineral chemical observations on the chromitites from the BOC. Our principal aims are to investigate the petrogenesis of chromitite in the BOC, elucidate the implications of chromitite formation for melt percolation in the palaeo-oceanic mantle preserved by the BOC, and to better constrain the setting(s) of partial mantle melting responsible for melt generation.

2. Geological setting

A thorough review of the different lithological components of the BOC and their contact relationships with each other has recently been published by Stone (2014). The BOC is exposed over an area of ~75 km^2 between Girvan and Ballantrae in south-west Ayrshire, Scotland (**Fig. 1**; Bonney, 1878; Church and Gayer, 1973; Stone and Smellie, 1988). The ophiolite was obducted onto the Laurentian margin during the closure of the Iapetus Ocean (i.e., the Grampian Orogeny; Church and Gayer, 1973; Bluck et al., 1980; Oliver et al., 2002; Power and Pirrie, 2004). Obduction is dated at 478 ±8 Ma, by K-Ar dating of amphibolite in the ophiolite sole (Bluck et al., 1980). The

complex is bound to the south by the Stinchar Valley Fault and unconformably overlain to the north by younger Llanvirn Barr and Caradoc-Ashgill Ardmillian Group sediments (Stone and Smellie, 1988; **Fig. 1**). Early work by Peach and Horne (1899), Pringle (1935), Bailey and McCallien (1952, 1957) and Church and Gayer (1973) attempted to explain the structural complexity of the BOC by invoking folding of the lava sequence, serpentinite intrusion and an anticlinal structure for the complex. Jones (1977) suggested that the BOC consists of a series of folded thrust sheets based on the lava sequence having uniform dips and strikes within each volcanic block, two compositionally distinct serpentinite belts and the observation that all lithological units appear to be fault-bounded.

The mantle portion of the BOC comprises variably serpentinised harzburgite and dunite which crop out in two broad NE-SW trending belts (**Fig. 1**; Stone and Smellie, 1988). The northern serpentinite belt is dominantly formed of harzburgite with lherzolite and minor pyroxenite (Jelínek et al., 1980, 1984; Stone and Smellie, 1988). It is metasomatised and preserves a strong tectonic fabric. By contrast, the southern serpentinite belt comprises harzburgite with dunite, wehrlite and minor troctolite (Stone and Smellie, 1988). The southern serpentinite is less metasomatised and locally exhibits a weak tectonic fabric. Chromitite has been documented in key localities in each of the serpentinite belts, at Pinbain Bridge and at Poundland Burn (**Fig.1**; Stone and Smellie, 1988) and these are the localities that concern the present study. It has been suggested that their lithological characteristics reflect formation of the southern serpentinite belt at a shallower depth than the northern belt (Stone, 2014 and references therein). A cumulate dunite sequence (i.e., a Moho transition zone; Boudier and Nicolas, 1995) has not been clearly distinguished in the BOC. The main masses of gabbro crop out at Millenderdale and from Byne Hill to Grey Hill (**Fig. 1**). The Millenderdale gabbros have been dated by K-Ar on amphibole, yielding an age of 487 ±8 Ma, and trondhjemite at Byne Hill has revealed a U-Pb zircon age of 483 ±4 Ma (Bluck et al., 1980). These gabbros exhibit intrusive relationships with their host rocks (Stone, 2014). The sheeted dyke complex in the BOC is represented at Duniewick Fort near Knockdolian, and possible poorly-developed elsewhere, e.g., at Millenderdale (**Fig. 1**; Oliver and McAlpine, 1998; Oliver et al.,

2002). The basalt lava sequences are exposed to the north of the northern serpentinite belt (Pinbain, Slockenray, Brandy Craig), between the serpentinite belts (Knockormal Hill, Moak Hill, Knockdaw Hill) and to the south of the southern serpentinite belt (Mains Hill, Craig Hill, Bargain Hill; **Fig. 1**).

3. Field observations at Poundland Burn and Pinbain Bridge

In the northern serpentinite belt at Pinbain Bridge, a sliver of structurally-fragmented and serpentinised harzburgite crops out in a sea cliff. The harzburgite contains small (0.2-0.5 cm; **Fig. 2a**) brown orthopyroxene pseudomorphs and abundant serpentinite (chrysotile) veining (~5 cm thick). A pervasively serpentinised, 4-5 m thick dunite lens occurs in the harzburgite and constitutes a broadly east-west trending zone that hosts poorly-defined lensoid chromitite bodies. The chromitite seams are characterised by variation in Cr-spinel abundance (from 60-95 vol.% Cr-spinel). Cr-spinel-rich dunites (containing 20-40 vol.% Cr-spinel) are also observed. The chromitite seams exhibit a range of thicknesses (from 5 cm to 0.5 mm). The northern margin of the chromitite band is marked by a brecciated fault zone that separates the chromitite from serpentinised harzburgite. Both harzburgite and dunite are commonly cross-cut by abundant ~5 cm thick fibrous chrysotile veins.

The chromitites and Cr-spinel-bearing peridotites at Poundland Burn in the southern serpentinite belt are enclosed in dunite lenses that are interlayered with harzburgite (see **Fig. S1**). Harzburgite is easily distinguished from dunite by the presence of randomly-oriented, brown orthopyroxene crystals (<0.5-1 cm in size), the majority of which have been pseudomorphed by bastite. Chromitites and Cr-spinel-bearing peridotites at Poundland Burn exhibit a range of textures, including well-developed nodular and anti-nodular varieties (**Figs. 2b,c**). Nodular-textured chromitite is characterised by 0.2-1.5 cm diameter sub-rounded, spheroidal to ellipsoidal Cr-spinel nodules in a serpentinised dunite groundmass (**Fig. 2b**). Where the nodules are ellipsoidal, several examples exhibit weak local alignments, but most are massive-textured. Variation in nodule packing is observed. The large (>1 cm) nodules are loosely-packed with the dunite groundmass

clearly distinguishable between individual nodules. However, as the Cr-spinel nodules decrease in size (from >1 to 0.2 cm), they exhibit closer-packing and a consequent decrease in groundmass proportion (i.e., from ~50 vol.% to ~30 vol.%; **Fig. S2**). Nodules tend to be locally very well sorted, in a given chromitite pod. However, size grading of Cr-spinel nodules from large (~1 cm) to small (<0.2 cm) is observed, with the largest nodules usually in the centres of the pods (see **Fig. S2** for different examples of different nodule sizes). Anti-nodular chromitite is also observed, formed of a dense Cr-spinel network enclosing small (<1 cm) spheroidal or ellipsoidal volumes of serpentinised dunite (**Fig. 2c**). The Cr- spinel crystals that form the network range from <1-0.5 mm in size. Between the different nodular and anti-nodular chromitite seams, the serpentinised dunites contain varying proportions of Cr-spinel as disseminated seams, clusters and accessory Cr-spinel crystals (**Fig. S1**). For example, rounded and elongate Cr-spinel clusters of <20 crystals in dunite are formed from Cr-spinel crystals ranging from <0.2-0.5 mm in size (**Fig. S2c**). Small Cr-spinel stringers (<5 cm long) and thin (<1 cm) seams are also present in the dunite units. The dunites transition to harzburgite gradationally (i.e., the boundaries between lithologies are not sharply defined) and often contain abundant magnetite veining. Harzburgite rarely contains Cr-spinel; if present, the Cr-spinel crystals occur in accessory proportions and are <0.2 cm in size.

4. Sample selection and analytical techniques

4.1 Sample selection

Sample selection was dictated to some extent by the poor degree of exposure and alteration of the BOC rocks. Only chromitites (Samples BA-10-03, BA-10-04) were analysed in detail from Pinbain Bridge, due to the high degrees of weathering and alteration of the peridotites there. Sample BA-10-03 is from a ~5 cm thick chromitite pod located towards the centre of the dunite lens at Pinbain Bridge, whereas BA-10-04 is from a thinner (~0.5 cm) close to the dunite-harzburgite contact. The Poundland Burn samples were collected at a poorly exposed outcrop at the head of Poundland Burn (see **Fig. S1**); samples of nodular chromitite (BA-10-06, BA-10-07), anti-nodular chromitite (BA-

10-10), Cr-spinel-rich dunite (BA-10-13) and dunite with accessory Cr-spinel (BA-10-11, BA-10-12) were selected for further analyses. Samples BA-10-06 and BA-10-07 are nodular-textured chromitite, sampled ~2 m away from one another (along strike, in the centre of the same seam). Sample BA-10-10 is an anti-nodular chromitite sampled ~20 m across strike from the nodular-textured chromitite that yielded BA-10-06 and BA-10-07. The relationships between BA-10-06/BA-10-07 and BA-10-10 are obscured by vegetative cover. Sample BA-10-13 was collected at the margin of the nodular-textured seam, and is a Cr-spinel rich dunite with a texture locally resembling that of anti-nodular chromitite, but with a greater proportion of silicate present. BA-10-11 and BA-10-12 are dunites from the envelope containing the main nodular-textured seam, and contain only accessory amounts of Cr-spinel.

4.2 Mineral chemistry by electron microprobe

A JEOL JXA-8900RL electron microprobe at the University of Göttingen (Germany) was employed to make backscatter electron micrographs and analyse the Cr-spinel/sulfide compositions from the two target chromitite localities. Analyses were conducted on both Cr-spinel crystal cores and sieve-textured alteration rims to enable compositions of both to be studied. Cr-spinel mineral chemical data were obtained using a 20.0 kV acceleration voltage, a 20 nA beam current and a 5 μm beam diameter with a 15 s peak count and 5 s background count for Mg, Al, Cr, Fe, Si and Mn and a 30 s peak count and 15 s background count for V, Ti, Ni and Zn. The standards were MgO, Al_2O_3, Cr_2O_3, TiO_2, NiO, V (synthetic), hematite for Fe, wollastonite for Si, rhodonite for Mn and gahnite for Zn. Ferric iron was calculated from the FeO content assuming perfect stoichiometry according to the method of Droop (1987). Sulphide grains situated in Cr-spinel alteration rims or adjacent to Cr-spinel crystals in the serpentinised groundmass were measured quantitatively using a 20.0 kV accelerating voltage, a 20 nA beam current and a 10 μm beam diameter. Larger sulphide grains (≥10 μm) were analysed with a 5 μm beam diameter. For sulphides, peak and background count times were 15 s and 5 s, respectively, for S, Fe and Zn, 30 s and 15 s peak and background, respectively, for As, Cu, Ni, Pb, Sb, and Co and 60 s and 30 s peak and background, respectively,

for Se and Te. Standards used were ZnS, AsGa, galena, gahnite and pure elements Te, Cu, Ni, Se, Sb, Fe and Co. Most sulphides were smaller than ~10 μm, so some were also analysed by EDS.

4.3 LA-ICP-MS trace elements

In situ trace element analysis was carried out by LA-ICP-MS at IGG-CNR, Pavia (Italy), using an Elan DRC-e quadrupole mass spectrometer coupled with a Q-switched Nd-YAG laser source (Quantel Brilliant). All of the LA-ICP-MS analyses were carried out on fresh Cr-spinel, away from grain boundaries and other textural features indicative of alteration. Sample ablation was carried out with a laser beam of 266 nm wavelength and a 60 μm spot size. Helium was used as carrier gas and mixed with Ar downstream of the ablation cell. NIST SRM 610 was used as external standard, while the Al content determined by EMPA was used as the internal standard. Precision and accuracy were assessed from repeated analyses of the BCR-2g and NIST SRM 612 standards, resulting in better than ±10% for concentrations at ppm levels. The LA-ICP-MS analysis was designed for the complete elemental characterisation of the spinels. It involved the concomitant acquisition of the signals of nearly 60 masses, encompassing major elements, REE, LILE, HFSE, Actinides, and most of the transitional elements relevant for the geochemical investigations. Detection limits were typically in the range of 100-500 ppb for Sc, 10-100 ppb for Sr, Zr, Ba, Gd and Pb, 1-10 ppb for Y, Nb, La, Ce, Nd, Sm, Eu, Dy, Er, Yb, Hf and Ta, and usually <1 ppb for Pr, Th and U. Further information about the analytical methods and data statistics employed is reported in Miller et al. (2012).

The electron microprobe Cr-spinel analyses carried out to reduce the LA-ICP-MS data were performed on a CAMECA-CAMEBAX microprobe at IGG-CNR (Istituto di Geoscienze e Georisorse-Consiglio Nazionale delle Ricerche), Padua, operating at 15 kV and 15 nA. A 20 s counting time was used for both peak and total background. Synthetic $MgCr_2O_4$ and $FeCr_2O_4$ spinels (Lenaz et al. 2004a) were used for Mg, Cr and Fe determination, Al_2O_3 for Al, $MnTiO_3$ for

Ti, and Mn, NiO for Ni and sphalerite for Zn. The raw data were reduced by a PAP-type correction software provided by CAMECA.

4.4 Single crystal X-ray diffraction

The combination of crystal structural parameters and mineral compositional data offers a potentially powerful way to evaluate Cr-spinel petrogenesis when combined with conventional mineral compositional microprobe data (cf. Lenaz et al., 2007). Eight representative Cr-spinel crystals (two from Pinbain Bridge and six from Poundland Burn) were separated from the BOC samples and analysed for their crystal structural characteristics using a KUMA-KM4 diffractometer (University of Trieste, Italy), using MoKα radiation and a monochromatised graphite crystal. Twenty-four equivalent reflections (12 8 4) or (8 4 4) were used depending on the size of the Cr-spinel crystal. Structural refinements were calculated using the SHELX-97 programme (Sheldrick, 1997) using the Fo^2_{hkl} in the *Fd-3m* space group. After X-ray data collection, the same crystals used for X-ray data collection were mounted on glass slides, polished and carbon coated for electron microprobe analyses on a CAMECA-CAMEBAX microprobe at IGG-CNR (Istituto di Geoscienze e Georisorse-Consiglio Nazionale delle Ricerche, Padua), using the procedures and standards utilised for the Padua electron microprobe analyses described in the previous section. T and M site cation distribution was calculated using the method described in Carbonin et al. (1996) and Lavina et al. (2002). The Cr-spinel compositions obtained for crystal structural analysis at the Padova electron microprobe are consistent with the Cr-spinel compositions analysed at the University of Göttingen (Germany). Intracrystalline closure temperatures for the BOC Cr-spinel crystals were calculated using the Princivalle et al. (1999) thermometer to provide insight into compositional changes occurring during Cr-spinel crystallisation and to elucidate their thermal history.

5. Results

5.1 Petrographic observations

The Cr-spinel contained in the Pinbain Bridge massive-textured chromitite seams consists of subhedral to euhedral crystals that range from 50-600 μm in size. The crystals are often highly-fractured and locally display alteration to Fe-rich thin replacement rims around their edges, manifested by their relatively bright appearance under back-scattered electrons (**Fig. 3a**). Fine-grained magnetite is locally associated with these rims. In some instances, the rims are developed up to ~2 μm thick. Towards the centres of seams, Cr-spinel crystals occur as massive aggregates with poorly defined crystal boundaries. Locally, where euhedral (polygonal) crystals occur within seams, they exhibit apparent (2D) dihedral angles of ~120˚ at Cr-spinel three-grain junctions, suggesting solid-state textural equilibration. The chromitite seam groundmass predominantly comprises mesh-textured serpentine pseudomorphs after olivine. Small (5-10 μm) irregularly-shaped sulphide grains occur in the serpentine groundmass and/or touching the altered rims at the edges of Cr-spinel crystals. More rarely, larger sulphide grains (>10 μm) are also observed, typically touching or close to Cr-spinel crystal edges. Fractures that cut through larger (100-200 μm) Cr-spinels (i.e., at the centres of seams) contain abundant small (<20 μm) Cr-spinel fragments (**Fig. 3b**). The majority of fractures that cut through Cr-spinel crystals are not associated with alteration of the Cr-spinel, suggesting they formed later, possibly in relation to the adjacent fault.

The Pinbain Bridge dunites hosting the chromitites are completely serpentinised, but rare olivine pseudomorphs are present. The harzburgites are also extensively serpentinised (~85-90 vol.%) but contain rare orthopyroxene pseudomorphs and accessory Cr-spinel (<1 %). Relict olivine crystal outlines are also observed in the harzburgite, ranging in size from 0.3-0.6 mm. The pseudomorphed orthopyroxene crystals, ranging between 200-700 μm in size, are replaced by bastite. Cr-spinel crystals (40-200 μm in size) are anhedral and sparsely distributed throughout the fine-grained serpentine groundmass. The groundmass exhibits a mesh texture and often contains thin, discontinuous veins of calcite and/or serpentine. The serpentine veins are composite, pointing towards repeated serpentinisation events.

The sub-rounded to elliptical chromitite nodules in the Poundland Burn chromitite seams locally display very thin and discontinuous Fe-rich alteration rims, though most nodules do not exhibit this feature at all (**Fig. 4**). Those nodules with the thickest alteration rims have irregular (i.e., non-rounded) nodule edges. The stepped edges referred to in Prichard et al. (2018) are observed on the edges of Cr-spinel nodules (**Fig. 4**). The alteration of Cr-spinel is confined to chromitite seam edges and is almost absent from the centres of chromitite seams. A small proportion of the Cr-spinel nodules have cores that contain silicate inclusions (mostly serpentine). A typical feature of the interiors of Cr-spinel nodules is the presence of cuspate-shaped areas filled with serpentine (**Figs. 3c, 4**), whereas the outer parts of nodules comprise massive Cr-spinel. Where two nodules are in contact, one may exhibit a concavity at its margin to accommodate the other, suggesting indentation. All of the nodules are moderately to heavily fractured. Cr-spinel crystals in finer grained nodular-textured seams also contain silicate inclusions (**Figs. 3c, 4a,c**). The fractures that cut through the Cr-spinel in the seams may or may not be associated with alteration of the Cr-spinel. The groundmass hosting the nodules consists of aggregates of fine-grained serpentine. Anti-nodular chromitite textures form a network of small (<100 μm) Cr-spinel crystals that surround (<1 mm diameter) rounded spheroids of serpentinised dunite. The Poundland Burn chromitites contain limited amounts of sulphides in the serpentinised groundmass, typically close to Cr-spinel alteration rims, or in Cr-spinel crystal fractures.

The Poundland Burn mantle peridotites comprise variably serpentinised harzburgite and dunite. Harzburgite contains large (<1 mm in size), randomly orientated, partially pseudomorphed orthopyroxene crystals. Where pseudomorphed, the orthopyroxene comprises bastite, mostly at the crystal edges and along cleavage planes (**Fig. 3d**). Olivine pseudomorphs, ranging from 0.2-1 mm in size, contain relict olivine domains partially replaced by a finer grained serpentine rim. The serpentinised groundmass has a reticulate texture, and rare, small (<20 μm) euhedral Cr-spinel crystals occur in the groundmass. The dunites contain euhedral to anhedral Cr-spinel crystals in small clusters and stringers of crystals, ranging from 50-400 μm in size (**Fig. 3e**). The abundance of

Cr-spinel in dunite is variable but generally higher than in harzburgite samples. Olivine pseudomorphs are typically less than 1 mm in size and are surrounded by thin magnetite veins. Isolated Cr- spinel crystals in dunite commonly have thicker Fe-rich replacement rims than those in the chromitites, which do not obscure primary stepped edges at crystal margins (**Fig. 3f**). Infrequently, Cr-spinel crystals contain rounded silicate inclusions in their cores, usually adjacent to fractures; this occurs in Cr-spinel crystals of all sizes, although it is generally found in larger Cr-spinels (**Fig. 3f**).

5.2 Cr-spinel and sulphide major element compositions

The electron microprobe analyses of the BOC chromitites (both fresh Cr-spinel cores and sieve-textured rims, as well as sulfides) are tabulated in the electronic supplement (*Table S1*). Generally, there is a marked bimodality in Cr-spinel composition between the two chromitite localities (**Fig. 5**). Poundland Burn chromitite Cr-spinels have relatively low Cr# (0.44-0.46), similar Mg# ([Mg/(Fe^{2+}+Mg)]; 0.52-0.77) values, and higher TiO_2 contents (0.21-0.27 wt.%) compared to the Pinbain Bridge chromitites overall (**Figs. 5a, 5b**). The Pinbain Bridge chromitites have moderately high Cr# (0.62-0.65), variable Mg# (0.54-0.70) and relatively low TiO_2 contents (0.08-0.12 wt.%). In particular, the nodular-textured chromitites analysed from Poundland Burn have a range of Cr# (0.44-0.45), Mg# (0.70-0.77) and TiO_2 (0.22-0.26 wt.%) that is distinct from the Pinbain Bridge chromitites. On plots of Cr# versus Mg# and TiO_2 versus Cr# (**Fig. 5**), the Poundland Burn Cr-spinel compositions mainly fall within the abyssal peridotite or MORB fields, and the Pinbain Bridge Cr-spinels (with higher Cr# and lower TiO_2) lie closer to (but mostly not within) the boninite field. Traverses across individual nodules in the Poundland Burn chromitite reveal that they are extremely homogenous with respect to their Cr, Al, Fe and Ti (**Fig. 4**) concentrations. Accessory Cr-spinels from Poundland Burn dunites exhibit more variable Cr# and Mg# values (0.42-0.49, 0.52-0.68, respectively) and TiO_2 contents (0.21-0.36 wt.%) than the chromitite Cr-spinels (Figs. 5. The discontinuous sieve-textured alteration rims on the Pinbain Bridge Cr-spinels

record moderate depletion in Mg^{2+} and Al^{3+} and enrichment in Cr^{3+} and Fe^{3+} at the crystal edges, so yield values toward the higher Cr# and TiO_2, and lower Mg# end of the ranges quoted above. Thin, highly discontinuous relatively Fe-rich rims on the Cr-spinels in the Poundland Burn dunites have Cr#: 0.37-0.47 and TiO_2: 0.19-0.39 wt.%, values similar to the Fe-rich rims in the Poundland Burn chromitite Cr-spinels (Cr#: 0.38-0.54; TiO_2: 0.17-0.29 wt.%).

The BOC chromitites contain only sparse base-metal sulphides (and platinum-group minerals; PGM). Where present, these grains are very small (~5 μm) situated either in Cr-spinel crystal cores or in the serpentinised groundmass. Three small (<3 μm) Ni-Fe-S grains were identified by EDS in the serpentinised groundmass adjacent to Cr-spinel crystals in the Pinbain Bridge chromitite. In this study, only one small (<2 μm) irarsite ([Ir,Ru,Rh,Pt]AsS) grain was documented at Pinbain Bridge. The nodular-textured chromitite from Poundland Burn contains several small sulphide grains (~10 μm) large enough for quantitative analysis. Five such sulphides were identified as heazlewoodite (Ni_3S_2) with minor Fe impurities (<1 wt. %) and one as millerite (NiS). Other small (<5 μm) sulphides identified by EDS in the Poundland Burn chromitites include Ni-S and Ni-Fe-S grains. No PGM were analysed from any of the Poundland Burn chromitites or associated dunites.

5.3 Cr-spinel trace element abundances

All of the LA-ICP-MS data are tabulated in the electronic supplement (*Table S2*), and only those elements with particular bearing on the petrogenetic interpretation are reported below. The trace element compositional variations in the BOC chromitites mirror the major element bimodality described above. For example, the Pinbain Bridge chromitite Cr-spinels have Sc contents that range from 5.1-6.6 ppm (n=7), V from 715-865 ppm, Mn from 1265-1654 ppm, Co from 218-243 ppm and Ga from 36-43 ppm. The Poundland Burn nodular chromitite Cr-spinels have Sc contents that range from 3-5 ppm (n=8), V from 889-929 ppm, Mn from 1156-1361 ppm, Co from 223-264 ppm and Ga from 54-60 ppm. By contrast, accessory Cr-spinel in dunite from Poundland Burn has Sc

contents that range from 1.3-6.2 ppm (n=6), V from 1033-1214 ppm, Mn from 1586-3071 ppm, Co from 358-474 ppm and Ga from 47.6-61.7 ppm. The relationships of V, Co and Ga with Cr# are shown in **Figures 6a, 6b** and **6c**, respectively, with the fields of trace element compositions of other (unpublished) UK ophiolite Cr-spinels shown for comparison. A well-developed negative correlation is noted between Ga and Cr#, in particular (**Fig. 6c**), when considered in light of the data from other ophiolites. Values for Cu, Ni and Zn are not as easily distinguished between the different Cr-spinel groups as the aforementioned elements, though a notable positive correlation is observed between Cu/Zn versus Cu/Ni for the whole population (**Fig. 6d**), possibly reflecting a sulfide control on these elements.

We have plotted the BOC Cr-spinel compositions on the spidergram of Pagé and Barnes (2009), which displays a range of important major and trace elements normalised to MORB (**Fig. 7**). The Poundland Burn Cr-spinels are similar to MORB with respect to their Ga, Ti, Ni, Zn and V abundances. They are relatively enriched in Co and Mn, and depleted in Sc, compared to MORB. In contrast, the Pinbain Bridge Cr-spinels are mildly depleted in Ga and Ni, and particularly in Ti, compared to MORB. They have similar abundances of Zn, V and Sc, and are enriched in Co and Mn, relative to MORB. Compared to boninite, BOC Cr-spinels are relatively enriched in Ga, Ti and Ni, similar in terms of Zn, Co and Mn abundances, and quite depleted with respect to V and Sc.

5.4 Crystal structural measurements

Cr-spinel crystals from Poundland Burn chromitites and Cr-spinel-bearing dunites have notably different cell edge lengths (a_0) and oxygen positional parameters (*u*) compared to the Cr-spinels in the Pinbain Bridge chromitites (*Table 1*, **Fig. 8**). It is worth highlighting that in spinel, the anions form a nearly cubic close-packed array, parallel to (111) planes, and the cations fill part of the tetrahedral (T) and octahedral (M) interstices available in the framework. Movement of the oxygen atom along the cube diagonal [111] causes the oxygen layers in the spinel structure to be slightly puckered so that variations in *u* correspond to displacements of the oxygens along the cube

diagonal, and reflect adjustments to the relative effective radii of cations in the tetrahedral and octahedral sites. An increase in *u* corresponds to an enlargement of the tetrahedral coordination polyhedra and a compensating decrease in the octahedra (Lindlsey, 1976). The Poundland Burn chromitite Cr-spinels display minimal variation in their a_0 and *u* values (8.2204-8.2285 Å and 0.2630-0.2634, respectively; **Fig. 8a**). Accessory Cr-spinel from Poundland Burn dunites displays longer cell edge lengths (a_0: 8.2456-8.2528 Å) and *u* values consistent with the other Poundland Burn chromitites (*u*: 0.2630-0.2631). Cr- spinel crystals from the Pinbain Bridge chromitites display the longest cell edge lengths (a_0: 8.2704- 8.2740 Å) and lowest *u* values (*u*: 0.2625). It is interesting to note that the Cr-spinels from Poundland Burn show the lowest cell edge lengths and the highest oxygen positional parameters amongst different ophiolite Cr-spinels analysed via X-ray single crystal diffraction reported to date (Shetland, a_0:8.26-8.31 Å; *u*: 0.2623-0.2631, Derbyshire et al., 2013; Oman, a_0: 8.24-8.29 Å; *u*: 0.2608-0.2629, Lenaz et al. 2014a; Albania, a_0: 8.27-8.31 Å; *u*: 0.2616-0.2627, Bosi et al., 2004; India, a_0: 8.28-8.30 Å; *u*: 0.2619-0.2623, Lenaz et al., 2014b). The data above suggest that even if a small amount of ferric iron (i.e., the alteration rims observed on some BOC Cr-spinels) was included in the single crystal analyses, the effects are negligible; the presence of a significant magnetite component would be expected to yield relatively low values of *u* (e.g., 0.2608-0.2612; Lenaz et al., 2014).

6. Discussion

6.1 Petrogenesis of nodular-textured and anti-nodular-textured chromitite in the BOC

Podiform chromitite has been documented from the mantle portions of numerous SSZ ophiolite complexes (Dick and Bullen, 1984; Arai, 1992; Melcher et al., 1997; Barnes and Roeder, 2001; Rollinson, 2008; Pagé and Barnes, 2009; Uysal et al., 2009; González-Jiménez et al., 2010, 2011; O'Driscoll et al. 2012a; Derbyshire et al., 2013; Arai and Miura, 2016). By contrast, ophiolites that do not have a SSZ provenance do not appear to ubiquitously develop chromitite (e.g., the Lizard, UK; Taitao, Chile; see also Rollinson and Adetunji (2013) and Arai and Miura (2015) for recent

discussion), suggesting that perhaps (hydrous) melt percolation in the supra-subduction mantle wedge is particularly conducive to their formation. The recognition that chromitite typically occurs within dunite envelopes in SSZ settings has led to widespread acceptance of melt-rock interaction mechanisms as fundamental processes for chromitite petrogenesis (Arai, 1992; 1997; Arai and Yurimoto, 1994; Zhou et al., 1996; Batanova et al., 2011; González-Jiménez et al., 2011; Derbyshire et al., 2013; González-Jiménez et al., 2014a, 2014b; Arai and Miura, 2016), following the classic work of Kelemen et al. (1990) and Kelemen et al. (1992; 1995). Field observations on the BOC chromitites therefore also implicate melt-rock interaction, in 'channels' of focused melt flow, as the key petrogenetic mechanism. This is because chromitite bodies in the BOC are ubiquitously hosted in dunite envelopes. Where visible (e.g., at Poundland Burn), harzburgite-dunite contacts are clearly defined and relatively sharp, although gradational boundaries are also present. Dunite lenses at Pinbain Bridge and Poundland Burn invariably contain more Cr-spinel than the host harzburgite. The abundance of Cr-spinel in dunite ranges from sparse clusters and stringers oriented parallel to the dunite-harzburgite contacts, to chromitite *sensu stricto*.

Nodular-textured chromitite is not ubiquitous in ophiolitic mantle, but has been documented in a number of cases worldwide including the Luobusa Ophiolite (Tibet; Zhou et al., 1996, 2001), the Kempirsai Massif (Kazakhstan; Melcher et al., 1997), the Troodos Ophiolite (Cyprus; Greenbaum, 1977) and the Semail Ophiolite (Oman; Ahmed and Arai, 2002; Rollinson and Adetunji, 2013; Zagrtdenov et al., 2018). Published nodular Cr-spinel analyses have been shown to display intermediate to high Cr# (0.60-0.86; Bilgrami, 1969; Greenbaum, 1977; Ahmed, 1982; Orberger et al., 1995; Vuollo et al., 1995; Zhou et al., 1996; Melcher et al., 1997; Ahmed and Arai, 2002; Morishita et al., 2006; Pagé and Barnes, 2009), considerably higher than those in the BOC (Cr#: ~0.45). The formation of nodular-textured chromitite is not well understood, although most workers have implicated physical processes (Arai and Miura, 2016), e.g., the coalescence of nodules in turbulent melt flow (Lago et al., 1982), magma mixing in melt flow conduits (Ballhaus, 1998) and melt-rock interaction (Zhou et al., 2001). Ballhaus (1998) showed that nodular chromitite

can form by the mingling of compositionally distinct melts in melt conduits. In his experiments, Ballhaus produced nodular chromitite remarkably similar to natural examples and his model proposes that each Cr-spinel nodule forms from incomplete mixing of a silica-poor melt (from deeper in the mantle) with a more siliceous melt (produced from melting of the harzburgite host). Matveev and Ballhaus (2002) expanded the work of Ballhaus (1998) to consider the effect of water on the formation of nodular chromitite, showing that the crystal-fluid and crystal-melt interfacial energies provide a control on Cr-spinel nodule formation. The Matveev and Ballhaus (2002) model proposes that fluid exsolved from a water-rich melt forms small bubbles that nucleate around dispersed Cr-spinel microphenocrysts contained within the melt. Due to the density contrast and differences in surface tension between the fluid bubbles and the melt, the Cr-spinel bearing fluid bubbles rise up the magma conduit and coalesce with other fluid bubbles to form a larger 'fluid pool' (Matveev and Ballhaus, 2002), an idea that may find support in recent experiments by Pleše et al. (2019). In a novel combined EBSD-X-ray microtomographic study, Prichard et al. (2015) reported that chromite nodules from the Troodos Ophiolite comprised a single skeletal crystal in their centres, surrounded by an outer mantle of polycrystalline chromite. The skeletal crystal at the nodule core crystallised from a chromite oversaturated melt, and Prichard et al. (2015) attributed the rounded smooth outer surfaces of nodules to dissolution by a chromite undersaturated melt, based on the observation that the outer boundaries of nodules truncate individual Cr-spinel crystal boundaries in the vicinity of the outer rim. One of the main implications of the Prichard et al. (2015) Troodos study is that the random growth-by-accumulation of chromite nodules in fluid bubbles within a turbulently-flowing melt, as per the Matveev and Ballhaus model, is not necessary.

In the BOC, the nodular chromitites are found in close proximity to anti-nodular textured chromitite. The Cr-spinel in anti-nodular-textured chromitite has an almost identical composition (Cr#: 0.44-0.46) to that of the adjacent nodular-textured chromitite. The *in situ* growth model of Prichard et al. (2015) does not easily account for the common existence of anti-nodular chromitite. However, the BOC nodules do exhibit some textural similarities with the Troodos examples, in that

silicate commonly occupies cuspate-shaped areas within the interiors of nodules (**Figs. 4**), and the outer mantles of nodules comprise massive-textured Cr-spinel. Rollinson and Adetunji (2013) also described this texture in a nodule from Maqsad, in the Oman Ophiolite (see their Figure 7), so it would seem that it is a common feature of nodular-textured chromitite. However, the BOC nodules have also undergone fracturing and deformation, obscuring some of the primary microstructure and making it difficult to positively identify Troodos-type skeletal intergrowths at the centres of nodules (if they exist). The relative compositional homogeneity of the nodular and anti-nodular chromitites combined with the lack of internal elemental zonation in individual nodules (**Fig. 4**) means that chemical evidence is not preserved for a process of magma mixing, as proposed by Ballhaus (1998). If magma mixing caused chromitite formation, then the mixing process must fortuitously have resulted in hybrid melts capable of crystallising Cr-spinel of very similar composition, despite the very different physical appearance of the nodular and anti-nodular textured chromitites. It has been noted by other studies that different chromitite textures may grade into each other, from massive textures in the centre of the chromitite pod through nodular Cr-spinel to anti-nodular and disseminated textures at the chromitite pod margin (Ahmed, 1982; Zhou et al., 1996, 2001; González-Jiménez et al., 2009, 2010; Marchesi et al., 2010; Borisova et al., 2012), suggesting a complex fluid dynamic regime. Unfortunately, a lack of exposure of the precise contact between the anti-nodular and nodular chromitites at Poundland Burn means that direct observation of the nature of the relationship between both is not possible. The nodular-textured chromitites at Poundland Burn rarely display any preferred alignment of nodules. However, indentation of nodules by one another is observed, pointing toward a degree of deformation in the conduit whilst the nodules were semi-crystalline, possibly at the post-accumulation stage.

In summary, the balance of evidence suggests that the Poundland Burn nodular chromitites formed in a conduit by melt-rock interaction, followed by a degree of flow (perhaps gravity-driven) sorting of the Cr-spinel nodules. Although we have not been able to verify the presence of skeletal crystals at the Cr-spinel nodule cores (Prichard et al. 2015), the stepped edges on Cr-spinel crystal

edges suggest Cr-spinel oversaturation in the melt conduit (**Figs. 3f, 4**). We interpret the cuspate areas of silicate minerals at the centres of most BOC Cr-spinel nodules as interstitial melt pockets between clusters of Cr-spinel crystals, subsequently overgrown by a massive-textured rim of chromitite. The observation that size-grading of nodules occurs within individual channels of the Poundland Burn chromitites may lend support for the model of Zhou et al. (2001), whereby changes in the fluid dynamic regime within the channel are responsible for a primary physical process such as 'snowballing'. One way that snowballing may be triggered in these channels is by the interaction of two immiscible liquids of differing viscosities (Joseph et al., 1984a, 1984b; Lemenand et al., 2003; Abarzhi, 2010; Abarzhi et al. 2005). In particular, the contrast is between the densities and viscosities of the ascending (H_2O-rich) basaltic melt (lower density and viscosity) and the siliceous melt produced from orthopyroxene dissolution in the harzburgitic host rock (higher density and viscosity) increases the Rayleigh-Taylor instability, promoting favourable conditions for faster melt velocities in the channel centres (Huppert and Sparks, 1985; Ballhaus, 1998; Gerya and Yuen, 2003; Herbert et al., 2009; Hack and Thompson, 2011). The largest (~1 cm) Cr-spinel nodules form in the centre of the melt channel where the melt flux is greatest, the availability of Cr is highest, and the degree of Cr-spinel oversaturation in the melt is at a maximum. Snowballing of the developing Cr-spinel nodules is therefore possible in the centre of the melt channel, facilitating the formation of larger nodules. With increasing proximity to the channel margin, the flow regime is more laminar, the melt flux and availability of Cr is lower, limiting the ability of the Cr-spinel nodule to snowball and thus restricting the nodule sizes. Our preferred model for formation of the nodular-textured chromitites at Poundland Burn therefore follows that of several recent authors working on these rocks (e.g., Prichard et al., 2015; 2018; O'Driscoll and González-Jiménez, 2016). Mass balance constraints (i.e., several 100s ppm Cr in the parental melt(s) versus 30-40 wt.% Cr_2O_3 in Cr-spinel) reflect concentration factors of 10^2-10^3 in each channel, so each chromitite body represents a high flux melt conduit that facilitated high degrees of melt-rock reaction and/or sustained melt throughflow over time in the upper mantle. The formation of nodular-textured chromitite in

particular requires the simultaneous presence in the melt channel of melts of different chemical composition and variation in the melt velocity profile across the channel. The relatively uniform major and trace element composition of the BOC nodular-textured (and anti-nodular) chromitite Cr-spinels studied here points to the effectiveness of individual channels in homogenising the signatures from the interacting melt compositions. A comparison of the BOC nodular-textured chromitite with those from the Troodos ophiolite suggests that the degree of Cr-spinel oversaturation achieved in the former was lower, but that the growth of the massive-textured rim to form the nodule outer portions was similar. An important future direction for the study of the BOC nodular chromitites will be a combined EBSD and X-ray microtomography study, with the principal aims of establishing whether the Cr-spinels in the rim have nucleated on those in the core, and whether or not there has been dissolution of grains at nodule margins, to verify the coupled oversaturation-driven crystallisation and dissolution model of Prichard et al. (2015) for these rocks.

6.2 Petrogenetic conditions and signatures of melt percolation in the BOC mantle

The compositional variation of Cr-spinel in ophiolite mantle sections has been shown to be a rich source of information on parental melt composition and the conditions of petrogenesis (cf. Dick and Bullen, 1984; Barnes and Roeder, 2001; Rollinson, 2008). In the BOC, the effects of late-stage alteration on Cr-spinel composition are relatively easy to diagnose in terms of physical appearance of crystals and compositional variation (e.g., intra-crystal fracturing, Fe-rich rims, scatter in rim compositions relative to fresh cores; **Fig. 5**). Primary Mg-Fe compostions in Cr-spinel can be affected by secondary processes, including subsolidus Mg^{2+}-Fe^{2+} exchange with surrounding silicates and even low temperature alteration (Barnes and Roeder, 2001). Given the extensive serpentinisation of the host peridotites at both the Pinbain Bridge and Poundland Burn localities, it is possible that some modification of primary Fe-Mg compositions has occurred in the chromitites, especially at crystal edges and close to alteration veins and intra-crystal fractures where visible alteration to Fe-rich spinel (ferroan Cr-spinel, magnetite) has occurred. **Figure 6d** suggests a sulfide control on Cu, Ni and Zn in the BOC chromitites which, given the relative paucity of sulfide present

in the rocks, might indicate that late-stage alteration has removed sulfide from the rocks. Similarly, accessory Cr-spinels from dunites and harzburgites are not considered to retain evidence of parental melt evolution. These crystals have probably extensively reequilibrated with the dominant surrounding silicate, as shown by their higher intracrystalline closure temperatures (see below). Therefore, we focus on the compositions of fresh Cr-spinel cores considered to be free from alteration and secondary modification in the following discussion. The distinct bimodality of Cr-spinel compositions observed between the two BOC localities is different to the continuous compositional trends observed from many SSZ ophiolite chromitites (Troodos Ophiolite, Büchl et al., 2004; Semail Ophiolite, Rollinson, 2005; and the Shetland Ophiolite Complex, Derbyshire et al., 2013), but has been documented from others as noted above. No intermediate Cr-spinel compositions have been found in the BOC, between the relatively aluminous Cr-spinels in the Poundland Burn chromitites (Cr#: 0.44-0.46) and the Cr-rich Cr-spinels in the Pinbain Bridge chromitites (Cr#: 0.62-0.65), suggesting that these two localities reflect percolation of melt with different chemical compositions and/or under different upper mantle environmental conditions. This point is also well illustrated by consideration of where the Cr-spinel populations from Pinbain Bridge and Poundland Burn group relative to one another on of Cr# versus Mg# and TiO_2 versus Al_2O_3 diagrams (**Fig. 5**). The Poundland Burn Cr-spinels plot in the MORB (abyssal peridotite) field in both instances, whereas the Pinbain Bridge Cr-spinels plot in or towards the island arc/boninite fields (**Fig. 5**).

The major element compositional differences between the Poundland Burn and Pinbain Bridge chromitites are also borne out in the trace element data. The Cr-spinels in the Pinbain Bridge chromitites have lower Al_2O_3, Ga, Ti and Ni, and generally higher Sc and Cr_2O_3, than the Poundland Burn chromitite Cr-spinels (**Fig. 7**). The Pinbain Bridge chromitites have higher Al_2O_3, Ga, Ti and Ni, and lower abundances V and Sc than boninite Cr-spinels. There are also differences between the Pinbain Bridge Cr-spinels and those from the Troodos arc picrite (i.e., lower Ti, higher Ni in the chromitite) although the other trace elements are present in similar abundances in each

(**Fig. 7**). The Poundland Burn chromitites have higher Zn, Mn and Co, and lower Sc than MORB Cr-spinels (**Fig. 7**). One general observation to be made from these comparisons is that the Pinbain Bridge Cr-spinels bear more resemblance to boninite Cr-spinels than the Poundland Burn chromitite Cr-spinels, and the Poundland Burn Cr-spinels are more similar to MORB Cr-spinels. However, the deviation of the BOC chromitites from ideal MORB or arc Cr-spinel compositions on **Figure 7** is also worth noting, in light of the complex melt-rock reaction processes invoked above for chromitite formation. Unlike crystallisation of Cr-spinel solely due to its saturation in a magma of a single composition, reaction between numerous batches of magma of different compositions with wall-rock peridotite that itself may vary in lithological composition/mineralogy has the potential to yield Cr-spinel compostions that are intermediate between ideal parental melt compositional types, as well as potentially incorporating component(s) from the host rock as well (i.e., from the breakdown of orthopyroxene). The melt-rock reaction model for chromitite formation therefore allows for the variation in Cr-spinel trace element compositions observed in the BOC, between both the Pinbain Bridge and Poundland Burn localities, and between the chromitites and the reference MORB, arc and boninite end member compositions.

Dare et al. (2009) introduced the $Ti/Fe^3\#$ versus $Ga/Fe^3\#$ diagram as a means of discriminating the tectonic setting and petrogenesis of Cr-spinels in mantle peridotites (**Fig. 9a**). Gallium is an interesting element for fingerprinting Cr-spinel petrogenesis because it occurs as a trivalent cation, so is unlikely to change during cooling and subsolidus processes, and is not known to be redox dependent, like Fe^{3+} (Dare et al., 2009). The diagram is principally for use with accessory Cr-spinels, as it has been calibrated (in terms of temperature of equilibration and olivine:spinel ratio) against oceanic and ophiolitic peridotite-bearing accessory spinels. Because of the importance of this calibration, there are limitations in its application to Cr-spinels from podiform chromitite (see Dare et al., 2009, for further discussion). However, our dataset includes measurements of accessory dunite-hosted Cr-spinel from Poundland Burn (Samples BA-10-11, BA-10-12), that fall within the 'peridotite field' of Dare et al. (2009) on the Cr# versus Mg# diagram

(**Fig. 5a**). It is interesting to note that these Cr-spinels fall mainly in the SSZ-reacted field or close to the MOR- and SSZ-reacted field boundary on the Ti/Fe^3# versus Ga/Fe^3# diagram (**Fig. 9a**), signifying formation by melt-rock reaction. The BOC chromitite analyses are included on the diagram for reference, but as noted by Dare et al. (2009), the fields they fall in may or may not reflect the petrogenetic conditions of formation. A field encompassing accessory Cr-spinels from the Lizard Ophiolite is included on **Figure 9a**, and points to a MORB setting for their crystallisation, in line with existing interpretations for that ophiolite (O'Driscoll et al., 2012b; Derbyshire, 2014).

The Cr-spinel crystal lattice can accommodate the substitution of cations (with different valences and ionic radii) and cation vacancies in the T and M sites (Lavina et al., 2002; Lenaz et al., 2004a, 2006; Juhin et al., 2007; Bosi et al., 2010; Fregola et al., 2011). Substitution of different cations forces the Cr-spinel crystal lattice to deform to accommodate the new cation by lattice relaxation and/or tilting of the cation sites (Juhin et al., 2007; Bosi et al., 2010; Hålenius et al., 2011). The spinel structure is non-convergent, displaying no change to the lattice symmetry between an ordered and disordered spinel (Harrison et al., 1999; Harrison and Putnis, 1999; Andreozzi et al., 2000; Nestola et al., 2007). The strong preference of Cr^{3+} for the M site can restrict the exchange of Mg and Al between the T and M sites (Lenaz et al., 2004b, 2010, 2012), resulting in a more ordered spinel structure (degree of inversion (x): 0 for ordered spinel, x: 1 for disordered spinel; Andreozzi et al., 2000; Nestola et al., 2007). Sack and Ghiorso (1991) showed that a completely random cation distribution between the T and M sites has an inversion value 'x': 2/3. The low inversion values determined for the BOC Cr-spinels (x: 0.14-0.21) using the Andreozzi et al. (2000) equation shows that they have a largely ordered cation distribution. The presence of large trivalent cations in the M site (e.g., Fe^{3+}, Cr^{3+}) modifies the octahedral angle and shared edge resulting in a lengthening of the T-O bond (Lavina et al., 2002). Lenaz et al. (2012) suggested that if the T-O bond is longer than the M-O bond, it indicates that a large cation is situated in the T site (e.g. Fe^{2+}). Octahedral distortion in Cr-spinel structure can be determined using the Bosi et al.

(2010) equation: $<\lambda_M> = 1.741 – 1.301(M\text{-}O/T\text{-}O) + 0.571(M\text{-}O/T\text{-}O)^2$ with a non-distorted octahedron having $<\lambda_M>$: 1. All of the BOC Cr-spinels display some distortion of the octahedron ($<\lambda_M>$: 1.010-1.013), overlapping with other ophiolite Cr-spinels ($<\lambda_M>$: 1.010-1.012; Bosi et al., 2004; **Fig. 8a**). The octahedral distortion in the Cr-spinel lattice directly affects the crystal stability in relation to changing parental melt composition, temperature and pressure (Bosi *et al.*, 2010). The Cr-spinel crystals from the Cr-rich Pinbain Bridge chromitites (Cr#: 0.62-0.65) have long cell edge lengths (*Table 1*), T-O bonds longer than their M-O bonds, distortion of the octahedral site and structural inversion (a_0: 8.2704-8.2740; T-O: 1.969-1.970; M-O: 1.964-1.9696; $<\lambda_M>$: 1.010-1.011; x: 0.20-0.21) that is associated with a relatively ordered Cr-spinel structure resulting from the relatively high abundance of Cr^{3+} restricting cation exchange between the T and M sites. The Al-rich Poundland Burn Cr-spinels (Cr#: 0.44-0.46) have shorter cell edge lengths, lower structural inversion and comparable octahedral site distortion than the Pinbain Bridge Cr-spinels (a_0: 8.2204-8.528; x: 0.14-0.18; $<\lambda_M>$: 1.012-1.013; *Table 1*). The T-O bond lengths in the Poundland Burn Cr-spinels correspond with Mg^{2+} being ordered in the T site (T-O bond length for Mg^{2+}: 1.965 Å, T-O bond length for Fe^{2+}: 1.997 Å; Lenaz et al., 2004a). The distortion to the octahedral site in the Poundland Burn Cr-spinel crystals ($<\lambda_M>$: 1.012-1.013) may not result from distortion in the tetrahedral site (Bosi et al., 2010), but may be attributed to varying the extent of Al^{3+} substitution for Cr^{3+} and Fe^{3+} in the M site. Therefore, the structural differences between the Cr-spinels from each locality may be a function of either compositional variation of the parental melt (controlling cation distribution by the availability and preference of Cr^{3+} for the M site; Princivalle et al., 1989; Lenaz et al., 2004b, 2010, 2012), or the rate of cooling (slow cooling facilitates cation ordering between the T and M sites; Princivalle et al., 1989; Uchida et al., 2005; Lenaz et al., 2012), or a combination of both factors.

Crystal structural analysis of Cr-spinels can provide insights into their thermal history by utilising *u* values, cation ordering and by determining intracrystalline closure temperatures (Princivalle et al., 1999; Uchida et al., 2005; Lenaz et al., 2010; 2011; 2012). Aluminium, Mg, Fe^{2+}

and Fe^{3+} do not have a strong site preference and are free to exchange between the octahedral and tetrahedral sites. On the other hand Cr, Ti and Ni favour the octahedral site, while Mn and Zn prefer the tetrahedral site (Lavina et al. 2002). The intracrystalline Mg – Al distribution between T and M sites of natural spinels mainly depends on the thermal history of the host rocks. When the cooling rate is slow, Mg and Al cations strongly order in T and M sites, respectively, whereas a faster cooling rate preserves a disordered cation distribution (Della Giusta *et al*. 1996; Princivalle *et al*. 1999). The geothermometer of Princivalle *et al*. (1999) takes into account the Mg- and Al-content of the Cr-spinels and their distribution across the octahedral and tetrahedral sites. The presence of other cations is accounted for by coefficients in the geothermometer equation. In general, the intracrystalline thermometer compares well with other (intercrystalline) geothermometers (e.g., olivine-spinel and two pyroxene thermometers; Lenaz et al. 2010; 2011). The intracrystalline thermometer may yield results lower than the aforementioned intercrystalline thermometers at higher *u*, but at lower *u* values (signifying a greater degree of cation disorder), good overlap is observed. For example, in a suite of Ronda peridotite (Spain) spinels, Lenaz et al. (2010; and references therein) found good agreement between the temperatures yielded by the intracrystalline thermometer and estimates from two-pyroxene- and olivine-spinel-based calculations.

Intracrystalline closure temperatures calculated for the BOC Cr-spinels plot away from values previously calculated for Shetland Ophiolite Complex and Albanian Ophiolite Cr-spinels (Derbyshire et al., 2013 and Bosi et al., 2004, respectively). The Cr-spinels from the Pinbain Bridge chromitites record closure temperatures of 793-853°C. The Poundland Burn nodular-textured and anti-nodular-textured chromitites reveal crystal closure temperatures of 623-708°C and 591°C, respectively. The Poundland Burn massive-textured chromitite yields a closure temperature of 630°C, falling within the nodular chromitite temperature range. Accessory Cr-spinel in dunite from Poundland Burn yields the highest range of closure temperatures (724-789°C); this is considered to be the result of secondary ordering and/or exchange of Al and Mg cations between Cr-spinel and other mineral phases (e.g., olivine; Lenaz et al., 2011; 2012). Small *u* values (<0.2625), cation

disorder between the T and M sites and higher intracrystalline closure temperatures are considered to indicate a relatively fast cooling rate (Princivalle et al., 1989; Della Giusta et al., 1996; Lenaz et al., 2012). Crystal structural analysis of the BOC chromitites shows that the group overall displays a limited range in *u* vales (0.2625-0.2634), a relatively ordered structure (x: 0.14-0.21) and moderate intracrystalline closure temperatures (591-853°C). The *u* parameter may also be controlled by changes in the bulk chemistry of the Cr-spinel crystal (specifically Cr^{3+}; Lenaz et al., 2007, 2010, 2011). The consistent Cr content (0.81-0.86 apfu) over the restricted *u* value range (*u*: 0.2629-0.2634) of the Poundland Burn Cr-spinels indicates that changes in bulk composition have not affected the *u* parameter. Instead, the *u* values are considered to reflect the cooling of the chromitites through their intracrystalline closure temperature(s). The lower end of the range of closure temperatures calculated here (591°C) is in good agreement with that of Cr-spinels in the Ronda peridotite (630°C; Lenaz et al. 2010) for similar u values, suggesting that this may indeed represent a lower bracket for Mg-Al exchange in mantle rocks. In contrast, the correlation between lowest *u* values and highest Cr content (*u*: 0.2625-0.2627; Cr#: 0.62-0.65; **Fig. 8,** *Table 1*) in the Pinbain Bridge Cr-spinels may result from changes to the bulk chemistry of the parental melt (increased Cr^{3+}). The low *u* and higher closure temperature range (793-853°C) indicates these Cr-spinels reached their intracrystalline temperature faster than those at Poundland Burn. It can be speculated that this might link to the exhumation of the northern serpentinite belt from deeper in the mantle than the southern belt, as has been proposed by other workers (Stone, 2014, and references therein).

We applied the algorithms of Rollinson (2008; adapted from Maurel and Maurel, 1982; Kamenetsky et al., 2001) to calculate the chromitite parental melt Al_2O_3 and TiO_2 compositions. The relationships are based on there being a linear relationship between the Al_2O_3 and TiO_2 content of Cr-spinel, and the Al_2O_3 and TiO_2 of the melt (Rollinson, 2008); in the case of MORB Cr-spinel-melt pairs a power law best-fit regression is obtained, and for arc Cr-spinel-melt pairs a logarithmic best describes the relationship. There is an implicit assumption that the Cr-spinels are in

equilibrium with their parental melt, which is likely to be an oversimplification given the complex processes operating in the melt channels described above, but the calculations are useful as a first step toward deciphering the tectonic setting in which the chromitites formed. For the Poundland Burn chromitites (that have relatively low Cr# values), the following expressions were applied:

$$Al_2O_3\text{-}melt = 7.1518 \times Al_2O_3\text{-}spinel^{0.2387}$$

$$TiO_2\text{-}melt = 1.5907 \times TiO_2spinel^{0.6322}$$

For the Pinbain Bridge chromitites, of likely arc affinity, the following equations were used:

$$Al_2O_3\text{-}melt = 5.2181 \times ln(Al_2O_3\text{-}spinel) - 1.0505$$

$$TiO_2\text{-}melt = 1.0963 \times TiO_2spinel^{0.7863}$$

The calculations were only carried out for fresh Cr-spinel cores analysed from each of the BOC chromitite localities, and reveal evidence of two compositionally distinct parental melts (**Fig. 9b**). The Pinbain Bridge parental melt is calculated to have had 13-14 wt. % Al_2O_3 and low TiO_2 contents (~0.2 wt. %), a composition similar to that of a boninitic melt (10.0-14.4 wt. % Al_2O_3; Maurel and Maurel, 1982; Kamenetsky et al., 2001; Pagé and Barnes, 2009; Uysal et al., 2009; Derbyshire et al., 2013). The Poundland Burn chromitites (including nodular-textured chromitite) yield higher Al_2O_3 (16-17 wt. %) and TiO_2 contents (0.55-0.75 wt. %) than the Pinbain Bridge chromitites indicating a MORB-like parental melt (MORB-like melt: >16 wt. % Al_2O_3). The calculations suggest the parental melts of the accessory Cr-spinels from the Poundland Burn dunites contained 15-16 wt. % Al_2O_3 and 0.3-0.5 wt. % TiO_2. Overall, the Poundland Burn chromitite and Cr-spinel bearing dunite parental melts plot within the MORB field whereas the Pinbain Bridge chromitite parental melts fall between the SSZ and MORB fields, suggesting formation of the latter by partial melting of a less depleted mantle source and/or lower degrees of partial melting, than required for melts in the arc field. The presence of I-PGE grains (laurite [RuS_2], erlichmannite [OsS_2], irarsite [IrAsS] and Ir-Os-Ru alloys; Power and Pirrie, 2004) in the Pinbain Bridge chromitites is a common feature of ophiolite chromitite, and may reflect the relatively high degrees of partial melting also suggested by the Pinbain Bridge Cr-spinel chemical compositions. The I-

PGE are compatible elements so occur in greater concentrations in higher degree partial melts (cf. Prichard et al., 1996; Melcher et al., 1997; Ahmed and Arai, 2002; Büchl et al., 2004; González-Jiménez et al., 2011). By contrast, Power and Pirrie (2004) found no PGM in the Poundland Burn chromitites. It is worth highlighting in the latter regard that Melcher et al. (1997) reported that their relatively high and low Cr# chromitites had contrasting PGM populations. Specifically, the low Cr# chromitites were deficient in Os-Ir alloys and primary inclusions more generally, an observation that Melcher et al. (1997) attributed to partial melting of a relatively fertile mantle source, in contrast to the more depleted SSZ mantle source from which the high Cr# chromitite parental melts derived. In addition, Uysal et al. (2009) found that while their relatively high Cr# (64-86) chromitites contained a rich inventory of PGM, their low Cr# (49-54) chromitite did not contain visible PGM at all. As with Melcher et al. (1997), Uysal et al. (2009) suggested that this reflected chromitite formation in MORB (low Cr#) versus SSZ (high Cr#) settings. In general, these observations support the inferences made from the parental melt calculations above; that the BOC chromitites formed from parental melts of different chemical composition.

6.3 Insights into the formation and tectonic setting of the BOC

The tectonic provenance of the BOC has been the subject of protracted debate (e.g., Wilkinson and Cann, 1974; Jones, 1977; Lewis and Bloxam, 1977; Thirlwall and Bluck, 1984; Stone and Smellie, 1988; Smellie and Stone, 1992, 2001; Smellie et al., 1995; Oliver and McAlpine, 1998; Stone, 2014). There are multiple reasons for this, amongst the most important are the lack of good inland exposure, the structurally fragmented nature of the complex and the contrasting trace element chemistry from the different basalt lava sequences. The BOC basalt lavas have trace element compositions ranging from MORB-like (LREE-depleted; Central Balcreuchan Group 3) to island arc tholeiite-like (LREE-enriched with a negative Nb + Ta anomaly; Central Balcreuchan Group 2, Southern Balcreuchan Group 1, Southern Balcreuchan Group 2), with two further lava blocks interpreted as exhibiting 'within-plate' signatures (LREE-enriched with high REE concentrations;

Northern Balcreuchan Group and Central Balcreuchan Group 1) (Wilkinson and Cann, 1974; Jones, 1977; Thirlwall and Bluck, 1984; Smellie and Stone, 2001). In addition, boninite signatures have been documented from the Games Loup lava sequence (Stone, 2014). Previously proposed tectonic settings for the BOC have therefore included within-plate (mantle plume-related; Wilkinson and Cann, 1974), a mid-ocean ridge (Jones, 1977) and an island arc associated with a back-arc basin (Bluck et al., 1980; Thirlwall and Bluck, 1984; Smellie and Stone, 1992, 2001; Smellie et al., 1995; Oliver and McAlpine, 1998; Armstrong et al., 1999). There has been a broad general consensus amongst many previous studies that the compositional disparity between the different lava blocks and gabbro units, the presence of arc-derived sediments situated beneath the lavas near Pinbain Hill (Smellie and Stone, 1992; Armstrong et al., 1999) and the MORB-like chemistry of the sheeted dyke complex (Oliver and McAlpine, 1998) point to an island arc setting with an associated back-arc basin prior to obduction of the BOC onto the Laurentian margin (Bluck et al., 1980; Thirlwall and Bluck, 1984; Smellie and Stone, 1992, 2001; Oliver and McAlpine, 1998; Armstrong et al., 1999). The formation of the back-arc basin supposedly resulted from the rifting of the Grampian arc, with the ophiolite representing the oceanward portion of the rifted arc and the back-arc basin (cf. Smellie and Stone, 1992, 2001). However, other workers have suggested alternating obduction/accretion events with basin filling and volcanism (Bluck, 1990; 2002).

The mantle portions of the BOC, as represented by the northern and southern serpentinite belts, are lithologically and chemically distinct from one another and therefore also contribute to the difficulty in invoking a single tectonic environment of formation for the BOC. The northern serpentinite contains a lithological assemblage and other characteristics consistent with it representing more depleted oceanic mantle than that preserved in the southern serpentinite belt (Stone, 2014). Broadly speaking, the presence of the bimodal chromitite compositions in the BOC permits at least two models for their formation. The first is a two-stage melting process that requires processing of the BOC mantle in different tectonic settings (i.e., MOR and SSZ; cf., Melcher et al., 1997; Ahmed and Arai, 2002; Uysal et al., 2009). The second explanation envisages all of the melt

percolation occurring above (or associated with) a developing subduction zone. In the latter case, it is possible that low Cr# chromitite could develop with incipient fore-arc (low degree) partial melting, with progression to higher Cr# chromitite as hydrous fluxing of the mantle wedge developed properly, analogous to the 'subduction initiation' geochemical evolution of ophiolite lava sequences proposed by Whattam and Stern (2011). Another option is that the low Cr# chromitite reflects melt percolation in the mantle below a back-arc spreading centre, simulating MORB-like melt depletion, which would necessarily be coeval with or postdate the high Cr# chromitite formation. Although imprecise, the chronological information available for the BOC points to the latter as being the more likely scenario. This is because the available geochronology (see Figure 7 in Stone 2014, and references therein) points to a significant temporal overlap between the arc and 'within-plate' lava sequences in the BOC. For example, ages of 476 ±14 Ma and 483 ±4 Ma (Sm-Nd isotope age in basalt and zircon U-Pb age from leucotonalite, respectively) for island arc magmatism are not distinguishable from ages of 470 ±10 Ma and 487 ±8 Ma for within plate magmatism (zircon U-Pb age from tuff, K-Ar age from gabbro, respectively). Whether fore-arc or back-arc, the characteristics of the Poundland Burn peridotite Cr-spinels on the Ti/Fe^{3}# versus Ga/Fe^{3}# diagram of Dare et al. (2009; **Fig. 9a**) and the fact that podiform chromitites are a rare-to-absent feature of MORB mantle (Rollinson and Adetunji, 2013) also support a subduction-related environment of formation for the dunite (and therefore the chromitite) channels, rather than a MORB setting.

One of the lines of support for magmatism in a back-arc setting comes from the presence of LREE-enriched lavas with high Zr/Nb, low Zr/Y ratios and high REE concentrations (Northern Balcreuchan Group at Pinbain, Slockenray, Brandy Craig and the Central Balcreuchan Group at Bennane Head). The Northern Balcreuchan Group and Central Balcreuchan Group 1 lavas display enrichments in the HFSE and REE and do not exhibit a negative Nb + Ta anomaly (Thirlwall and Bluck, 1984; Smellie and Stone, 2001). Interestingly, the apparent absence of a Nb depletion signature in some arc lavas and tuffs from the Aeolian arc (southern Italy), the Aegean arc (Greece)

and in western Ireland as observed, for example, by Clift and Blusztajn (1999) and Draut and Clift (2001), has been attributed to the slowing and termination of subduction. The LREE-enriched Northern Balcreuchan Group and Central Balcreuchan Group 1 lavas might therefore represent late-stage melts formed during the slowing and eventual termination of the southward subduction before the subduction polarity reversal after the accretion of the Grampian arc (Dewey and Ryan, 1990; Ryan and Dewey, 1991; Oliver et al., 2002; Strachan et al., 2002; Dewey, 2005; MacDonald and Fettes, 2006). The slowing of subduction would restrict the amount of fluid available for fluxing the mantle wedge thus lowering the degree of partial melting. The resulting melt would be enriched in LILE, HFSE and LREE, but would also generate chromitite with lower Cr#, offering a plausible scenario for the petrogenesis of the Poundland Burn chromitites forming in the mantle beneath a back-arc spreading centre.

7. Summary and Conclusions

Although obscured to a degree by late-stage faulting and secondary alteration (serpentinisation), the Ballantrae Ophiolite Complex preserves evidence for melt extraction and percolation in a SSZ environment. The Pinbain Bridge and Poundland Burn chromitites formed by melt-rock reaction in channel-like conduits in the upper mantle. Although the formation of nodular-textured chromitite in ophiolitic mantle is generally not well understood (Arai and Miura, 2016), the BOC examples have textural and lithological similarities to those reported from other ophiolites (including Oman and Troodos). This suggests a common mechanism of formation and, looking forward, new constraints on their petrogenesis may result from the application of the X-ray microtomography technique of Prichard et al. (2015) to test for an origin by Cr-spinel oversaturation in the melt and *in situ* crystallisation.

The petrological differences previously documented between the northern and southern serpentinite limbs of the BOC are reflected in the chemical compositions of chromitite Cr-spinel from each. The presence of high-Cr# (Pinbain Bridge) and low Cr# (Poundland Burn) chromitites suggests that either the Ballantrae mantle section preserves evidence for melt extraction at both a

MOR and in a SSZ setting, or the contrasting chromitite compositions reflect progressive changes in the compositions of the parental melts (and hence the style of melt extraction) in a complex subduction zone setting. Our combined datasets and observations suggest that the latter scenario is more likely, and the trace element characteristics (i.e., $Ti/Fe^3\#$ versus $Ga/Fe^3\#$ systematics) of accessory Cr-spinel formed in dunite at Poundland Burn (i.e., illustrated in **Fig. 9a**) serve to support this inference. Given the diversity of basalt compositions associated with the BOC (cf. Stone, 2014), the contrasting signatures preserved in the chromitites provide a useful dimension to aiding interpretation of the environment of formation of the ophiolite, as well as highlighting more generally the utility of mantle-hosted chromitites as for finger-printing melt percolation and melt-rock reaction.

Acknowledgements

The work in this paper forms part of the PhD research carried out by EJ Derbyshire at Keele University (Derbyshire, 2014). Funding for the work presented in this article was received by EJD from the Edinburgh Geological Society, the EPSAM Research Institute (Keele University) and the Keele Postgraduate Association (Keele University) and is gratefully acknowledged. Andreas Kronz is thanked for for assistance with electron-microprobe analyses at the University of Göttingen. Funding for the trace element analysis of Cr-spinels was provided to DL by the University of Trieste (FRA2009). B.O'D. acknowledges support from a Royal Society Research Grant (RG100528) and from Natural Environment Research Council (NERC) New Investigator grant NE/J00457X/1 whilst based at Keele University. Peter Greatbatch and Dave Wilde are acknowledged for their excellent thin-section production. Hugh Rollinson and an anonymous reviewer are thanked for their detailed comments, which greatly improved an earlier version of the manuscript, as did the editorial suggestions of Andrew Kerr.

References

Abarzhi, S., 2010. On fundamentals of Rayleigh-Taylor turbulent mixing. EPL (Europhysics Letters) 91(3), 35001.

Abarzhi, S., Gorobets, A. and Sreenivasan, KR., 2005. Rayleigh-Taylor turbulent mixing of immiscible, miscible and stratified fluids. Physics of Fluids 17(8), 081705.

Ahmed, Z., 1982. Prophyritic-nodular, nodular and orbicular chrome ores from the Sakhakot-Qila complex Pakistan, and their chemical variations. Mineralogical Magazine 45, 167-178.

Ahmed, A. H., Arai, S., 2002. Unexpectedly high-PGE chromitite from the deeper mantle section of the northern Oman ophiolite and its tectonic implications. Contributions to Mineralogy and Petrology 143, 263-278.

Andreozzi, G. B., Princivalle, F., Skogby, H., Della Giusta, A., 2000. Cation ordering and structural variation with temperature in MgAl2O4 spinel: an X-ray single crystal study. American Mineralogist 85, 1164-1171.

Arai, S., 1992. Chemistry of chromian spinel in volcanic rocks as a potential guide to magma chemistry. Mineralogical Magazine 56, 173-184.

Arai, S., 1997. Control of wall-rock composition on the formation of podiform chromitites as a result of magma/peridotite interaction. Resource Geology 47, 177-187.

Arai, S., Yurimoto, H., 1994. Podiform chromitites of the Tari-Misaka Ultramafic Complex, Southern Japan, as mantle-melt interaction products. Economic Geology 89, 1279-1288.

Arai, S., Miura, M., 2015. Podiform chromitites do form beneath mid-ocean ridges. Lithos 232, 143-149.

Arai, S. and Miura, M., 2016. Formation and modification of chromitites in the mantle. Lithos 264, 277-295.

Armstrong, H. A., Owen, A. W., Floyd, J. D., 1999. Rare earth geochemistry of Arenig cherts from the Ballantrae Ophiolite and Leadhills Imbricate Zone, southern Scotland: implications for origin and significance to the Caledonian orogeny. Journal of the Geological Society 156, 549-560.

Bailey, E. B., McCallien, W. J., 1952. Ballantrae problems: a historical review. Transactions of the Edinburgh Geological Society 15, 14-38.

Bailey, E. B., McCallien, W. J., 1957. The Ballantrae Serpentine, Ayrshire. Transactions of the Edinburgh Geological Society 17, 33-53.

Ballhaus, C., 1998. Origin of podiform chromite deposits by magma mingling. Earth and Planetary Science Letters 156, 185-193.

Barnes, S. J., Roeder, P., 2001. The range of spinel compositions in terrestrial mafic and ultramafic rocks. Journal of Petrology 42, 2279–2302.

Batanova, V. G., Belousov, I. A., Savelieva, G. N., Sobolev, A. V., 2011. Consequences of channelized and diffuse melt transport in supra-subduction zone mantle: Evidence from the Voykar Ophiolite (Polar Urals). Journal of Petrology 52, 2483-2521.

Bédard, J. H., Hébert, R., 1998. Formation of chromitites by assimilation of crustal pyroxenites and gabbros into peridotitic intrusions: North Arm Mountain Massif, Bay of Islands ophiolite, Newfoundland, Canada. Journal of Geophysical Research 103(B3), 5165-5184.

Bilgrami, S. A., 1969. Geology and chemical mineralogy of the Zhob Valley chromite deposits, west Pakistan. The American Mineralogist 54, 134-148.

Bluck, B. J., 1990. Terrane provenance and amalgamation: examples from the Caledonides. Philosophical Transactions of the Royal Society of London, Series A, Mathematical and Physical Sciences 331, 599-609.

Bluck, B. J., 2002. The midland Valley terrane, in: Trewin, N. H. (Ed.), The Geology of Scotland (2nd Edition). The Geological Society, London, pp. 167-200.

Bluck, B. J., Halliday, A. N., Aftalion, M., MacIntyre, R. M., 1980. Age and origin of Ballantrae ophiolite and its significance to the Caledonian Orogeny and Ordovician time scale. Geology 8, 492-495.

Bonney, T. G., 1878. On the serpentine and associated igneous rocks of the Ayrshire coast. Quarterly Journal of the Geological Society 34, 769-785.

Borisova, A. Y., Ceuleneer, G., Kamenetsky, V. S., Arai, S., Bénjina, F., Abily, B., Bindeman, I. N., Polvé, M., de Parseval, P., Aigouy, T., Pokrovski, G. S., 2012. A new view on the petrogenesis of the Oman Ophiolite chromitites from microanalyses of chromite-hosted inclusions. Journal of Petrology 53, 2411-2440.

Bosi, F., Andreozzi, G., Ferrini, V., Lucchesi, S., 2004. Behaviour of cation vacancy in kenotetrahedral Cr-spinels from Albanian eastern belt ophiolites. American Mineralogist 89, 1367–1373.

Bosi, F., Hålenius, U., Skogby, H., 2010. Crystal chemistry of the MgAl2O4-MgMn2O4-MnMn2O4 system: analysis of structural distortion in spinel- and hausmannite-type structures. American Mineralogist 95, 602-607.

Boudier, F., Nicolas, A., 1995. Nature of the Moho Transition Zone in the Oman Ophiolite. Journal of Petrology 36, 777-796.

Büchl, A., Brügmann, G. E., Batanova, V. G., 2004. Formation of podiform chromitite deposits: implications from PGE abundances and Os isotopic compositions of chromites from the Troodos complex, Cyprus. Chemical Geology 208, 217-232.

Carbonin, S., Russo, U., Della Giusta, A., 1996. Cation distribution in some natural spinels from X-ray diffraction and Mössbauer spectroscopy. Mineralogical Magazine 60, 355-368.

Church, W. R., Gayer, R. A., 1973. The Ballantrae Ophiolite. Geological Magazine 110, 497-510.

Clift, P., Blusztajn, J., 1999. The trace-element characteristics of Aegean and Aeolian volcanic arc marine tephra. Journal of Volcanology and Geothermal Research 92, 321-347.

Dare, S. A. S., Pearce, J. A., McDonald, I., Styles, M. T., 2009. Tectonic discrimination of peridotites using fO2-Cr# and Ga-Ti-FeIII systematics in chrome-spinel. Chemical Geology 261, 199–216.

Della Giusta, A., Carbonin, S., Ottonello, G., 1996. Temperature-dependent disorder in a natural Mg-Al-Fe2+-Fe3+-spinel. Mineralogical Magazine 60, 603-616.

Derbyshire, E. J., 2014. Upper mantle processes, serpentinisation and late-stage alteration preserved in British ophiolite peridotites and chromitites. PhD Thesis, Keele University, UK, 236 pp

Derbyshire, E.J., O'Driscoll, B., Lenaz, D., Gertisser, R., Kronz, A., 2013. Compositionally heterogeneous podiform chromitite in the Shetland Ophiolite Complex (Scotland): implications for chromitite petrogenesis and late-stage alteration in the upper mantle portion of a supra-subduction zone ophiolite. *Lithos*, 162-163, 279-300.

Dewey, J. F., 2005. Orogeny can be very short. Proceedings of the National Academy of Sciences of the United States of America 102, 15286-15293.

Dewey, J. F., Ryan, P. D., 1990. The Ordovician evolution of the South Mayo trough, western Ireland. Tectonics 9, 887-902.

Dick, H. J. B., Bullen, T., 1984. Chromium-spinel as a petrogenetic indicator in abyssal and alpine-type peridotites and spatially associated lavas. Contributions to Mineral Petrology 86, 54-76.

Draut, A. E., Clift, P. D., 2001. Geochemical evolution of arc magmatism during arc continent collision, South Mayo, Ireland. Geology 29, 543-546.

Droop, G. T. R., 1987. A general equation for estimating Fe 3+ concentrations in ferromagnesian silicates and oxides from microprobe analyses, using stoichiometric criteria. Mineralogical Magazine 51, 431-435.

Fregola, R. A., Bosi, F., Skogby, H., 2011. A first report on anion vacancies in a defect $MgAl_2O_4$ natural spinel. Periodico di Mineraligia 80, 27-38.

Gerya, T, V., Yuen, D. A., 2003. Rayleigh-Taylor instabilities from hydration and melting propel 'cold plumes' at subduction zone. Earth and Planetary Science Letters 212, 47-62.

González-Jiménez, J. M., Kerestedjian, T., Proenza, J. A., Gervilla, F., 2009. Metamorphism on chromite ores from the Dobromirtsi Ultramafic Massif, Rhodope Mountains (SE Bulgaria). Geologica Acta 7, 413-429.

González-Jiménez, J. M., Gervilla, F., Kerestedjian, T., Proenza, J. A., 2010. Alteration of Platinum-group and Base- Metal mineral assemblages in ophiolite chromitites from the Dobromirtsi Massif, Rhodope Mountains (Bulgaria). Resource Geology 60, 315-334.

González-Jiménez, J. M., Proenza, J. A., Gervilla, F., Melgarejo, J. C., Blanco-Moreno, J. A., Ruiz-Sanchez, R., Griffin, W. L., 2011. High-Cr and high-Al chromitites from the Sagua de Tánamo district, Mayarí-Cristal ophiolitic massif (eastern Cuba): Constraints on their origin from mineralogy and geochemistry of chromian spinel and platinum-group elements. Lithos 125, 101 121.

González-Jiménez, J.M., Griffin, W.L., Gervilla, F., Proenza, J.A., O'Reilly, S.Y., Pearson, N.J., 2014a. Chromitites in ophiolites: how, where, when, why? Part I. Origin and significance of platinum-group minerals. Lithos 189, 127–139

González-Jiménez, J.M., Griffin, W.L., Proenza, J.A., Gervilla, F., O'Reilly, S.Y., Akbulut, M., Pearson, N.J., Arai, S., 2014b. Chromitites in ophiolites: how, where, when, why? Part II. The crystallisation of chromitites. Lithos 189, 140–158

Greenbaum, D., 1977. The chromitiferous rocks of the Troodos Ophiolite Complex, Cyprus. Economic Geology 72, 1175-1194.

Hack, A. C., Thompson, A. B., 2011. Density and viscosity of hydrous magmas and related fluids and their role in subduction zone processes. Journal of Petrology 52, 1333-1362.

Hålenius, U., Bosi, F., Skogby, H., 2011. A first record of strong structural relaxation of TO4 tetrahedra in a spinel solid solution. American Mineralogist 96, 617-622.

Harrison, R. J., Putnis, A., 1999. Determination of the mechanism of cation ordering in magnesioferrite (MgFe2O4) from the time- and temperature-dependence of magnetic susceptibility. Physics and Chemistry of Minerals 26, 322-332.

Harrison, R. J., Dove, M. T., Knight, K. S., Putnis, A., 1999. In-situ neuron diffraction study of non-convergent cation ordering in the (Fe3O4)1-x(MgAl2O4)x spinel solid solution. American Mineralogist 84, 555-563.

Herbert, L. B., Antoshechkina, P., Asimow, P., Gurnis, M., 2009. Emergence of a low viscosity channel in subduction zones through the coupling of mantle flow and thermodynamics. Earth and Planetary Science Letters 278, 243-256.

Hunt, E., O'Driscoll, B., Daly, J.S., 2012. Parental magma composition of the syn-tectonic Dawros Peridotite chromitites, NW Connemara, Ireland. Geological Magazine, 149(4), 590-605.

Huppert, H. E., Sparks, R. S. J., 1985. Cooling and contamination of mafic and ultramafic magmas during ascent through continental crust. Earth and Planetary Science Letters 74, 371-386.

Jelínek, E., Soucek, J., Bluck, B. J., Bowes, D. R., Treloar, P. J., 1980. Nature and significance of beerbachites in the Ballantrae ophiolite, SW Scotland. Transactions of the Royal Society of Edinburgh: Earth Sciences 71, 159-179.

Jelínek, E., Soucek, J., Randa, Z., Jakeš, P., Bluck, B. J., Bowes, D. R., 1984. Geochemistry of peridotites, gabbros and trondhjemites of the Ballantrae complex, SW Scotland. Transactions of the Royal Society of Edinburgh: Earth Sciences 75, 193-209.

Jones, C. M., 1977. The Ballantrae Complex as compared to the ophiolites of Newfoundland. Unpublished Ph. D thesis, Cardiff University.

Joseph, D. D., Renardy, M., Renardy, Y., 1984a. Instability of the flow of two immiscible liquids with different viscosities in a pipe. Journal of Fluid Mechanics 141, 309- 317.

Joseph, D. D., Nguyen, K., Beavers, G. S., 1984b. Non-uniqueness and stability of the configuration of flow of immiscible fluids with different viscosities. Journal of Fluid Mechanics 141, 319-345.

Juhin, A., Calas, G., Cabaret, D., Galoisy, L., Hazemann, J-L., 2007. Structural relaxation around substitutional Cr3+ in MgAl2O4. Physical Review B 76, doi:10.1103/PhysRevB.76.054105

Kamenetsky, V. S., Crawford, A. J., Meffre, S., 2001. Factors controlling chemistry of magmatic spinel: an empirical study of associated olivine, Cr-spinel and melt inclusions from primitive rocks. Journal of Petrology 42, 655–671.

Kelemen, P. B., Johnson, K. T. M., Kinzler, R. J., Irving, A. J., 1990. High-field-strength element depletions in arc basalts due to mantle-magma interaction. Nature 345, 521-524.

Kelemen, P. B., Dick, H. J. B., Quick, J. E., 1992. Formation of harzburgite by pervasive melt/rock interaction in the upper mantle. Nature 358, 365-641.

Kelemen, P. B., Shimizu, N., Salters, V. J. M., 1995. Extraction of mid-ocean ridge basalt from the upwelling mantle by focused flow of melt in dunite channels. Nature 375, 747-753.

Kepezhinskas, P. K., Taylor, R. N. & Tanaka, H., 1993. Geochemistry of plutonic spinels from the north Kamchatka arc: comparisons with spinels from other tectonic settings. Mineralogy Magazine 57, 575-589.

Kovács, G. P., Buda, G., Watkinson, D. H., Tompa, L., 1997. Chromite deposits of the Sagua-Baracoa range, Eastern Cuba. Acta Geologica Hungarica 40, 337-353.

Lago, B. L., Rabinowicz, M., Nicolas, A., 1982. Podiform chromite ore bodies: a genetic model. Journal of Petrology 23, 103-125.

Lavina, B., Salviulo, G., Della Guista, A., 2002. Cation distribution and structural modelling of spinel solid solutions. Physics and Chemistry of Minerals 29, 10-18.

Lemenand, T., Della Valle, D., Zellouf, Y., Peerhossaini, H., 2003. Droplets formation in turbulent mixing of two immiscible fluids in a new type of static mixer. International Journal of Multiphase Flow 29, 813-840.

Lenaz, D., Skogby, H., Princivalle, F., Hålenius, U., 2004a. Structural changes and valence states in the $MgCr_2O_4$ - $FeCr_2O_4$ solid solution series. Physics and Chemistry of Minerals 31, 633-642.

Lenaz, D., Andreozzi, G. B., Mitra, S., Bidyananda, M., Princivalle, F., 2004b. Crystal chemical and 57Fe Mössbauer study of chromite from the Nuggihalli schist belt (India). Mineralogy and Petrology 80, 45-57.

Lenaz, D., Skogby, H., Princivalle, F., Hålenius, U., 2006. The MgCr2O4-MgFe2O4 solid solution series: effects of octahedrally coordinated Fe3+ on T-O bond lengths, Physics and Chemistry of Minerals 33, 465-474.

Lenaz, D., Braidotti, R., Princivalle, F., Garuti, G., Zaccarini, F., 2007. Crystal chemistry and structural refinements of chromites from different chromitite layers and xenoliths of the Bushveld Complex. European Journal of Mineralogy 19, 599-609.

Lenaz, D., De Min, A., Garuti, G., Zaccarini, F., Princivalle, F., 2010. Crystal chemistry of Cr-spinels from the lherzolite mantle peridotite of Ronda (Spain). American Mineralogist 95, 1323–1328.

Lenaz, D., O'Driscoll, B., Princivalle, F., 2011. Petrogenesis of the anorthosite-chromitite association: crystal-chemical and petrological insights from the Rum Layered Suite, NW Scotland. Contributions to Mineralogy and Petrology 162, 1201-1213.

Lenaz, D., Garuti, G., Zaccarini, F., Cooper, R. W., Princivalle, F., 2012. The Stillwater Complex chromitites: the response of chromite crystal chemistry to magma injection. Geologica Acta 10, 33-41.

Lenaz, D., Adetunji, J., Rollinson, H., 2014a. Determination of $Fe^{3+}/\Sigma Fe$ ratios in chrome spinels using a combined Mössbauer and single-crystal X-ray approach: application to chromitites from the mantle section of the Oman ophiolite. Contributions to Mineralogy and Petrology 167, article 958.

Lenaz, D., Andreozzi, G.B., Bidyananda, M., Princivalle, F., 2014b. Oxidation degree of chromite from Indian ophiolites: a crystal chemical and ^{57}Fe Mössbauer study. Periodico di Mineralogia 83, 241-255,

Lewis, A. D., Bloxam, T. W., 1977. Petrotectonic environments of the Girvan-Ballantrae lavas from rare-earth element distributions. Scottish Journal of Geology 13, 211-222.

Lindsley, D.H., 1976. The crystal chemistry and structure of oxide minerals as exemplified by the Fe-Ti oxides. In Rumble III D (Ed), Rev Mineral 3:L1-L60.

Maaløe, S., 2005. The dunite bodies, websterite and orthopyroxenite dikes of the Leka Ophiolite Complex, Norway. Mineralogy and Petrology 85, 163–204.

MacDonald, R., Fettes, D. J., 2006. The tectonomagmatic evolution of Scotland. Transactions of the Royal Society of Edinburgh: Earth Sciences 97, 213-295.

Marchesi, C., González-Jiménez, J. M., Gervilla, F., Garrido, C. J., Griffin, W. L., O'Reilly, S. Y., Proenza, J. A., Pearson, N. J., 2010. In situ Re-Os isotopic analysis of platinum-group minerals from the Mayari-Cristal ophiolitic massif (Mayari-Baracoa ophiolitic belt, eastern Cuba): implications for the origin of Osisotope heterogeneities in podiform chromitites. Contributions to Mineralogy and Petrology 161, 977-990.

Matveev, S., Ballhaus, C., 2002. Role of water in the origin of podiform chromitite deposits. Earth and Planetary Science Letters 203, 235-243.

Maurel, C., Maurel, P., 1982. Etude expérimentale de la distribution de l'aluminium entre bain silicaté basique et spinelle chromifère. Implications pétrogénétiques: teneur en chrome des spinelles. Bulletin de Minéralogie 105, 197-202.

Melcher, F., Grum, W., Simon, G., Thalhammer, T. V., Stumpfl, E. F., 1997. Petrogenesis of the Ophiolitic Giant Chromite Deposits of Kempirsai , Kazakhstan: a study of solid and fluid inclusions in chromite. Journal of Petrology 38, 1419-1458.

Miller, C., Zanetti, A., Thöni, M., Konzett, J., Klötzli, U., 2012. Mafic and silica-rich glasses in mantle xenoliths from Wau-en-Namus, Libya: textural and geochemical evidence for peridotite-melt reactions. Lithos 128-131, 11-26.

Morishita, T., Andal, E. S., Arai. S., Ishida, Y., 2006. Podiform chromitites in the lherzolite-dominant mantle section of the Isobela ophiolite, the Philippines. Island Arc 15, 84-101.

Nestola, F., Ballaran, T. B., Balic-Zunic, T., Princivalle, F., Secco, L., Dal Negro, A., 2007. Comparative compressibility and structural behaviour of spinel MgAl2O4 at high pressures: the independency on the degree of cation order. American Mineralogist 92, 1838-1843.

O'Driscoll, B., Day, J. M. D., Walker, R. J., Daly, J. S., McDonough, W. F., Piccoli, P. M., 2012a. Chemical heterogeneity in the upper mantle recorded by peridotites and chromitites from the Shetland Ophiolite Complex, Scotland. Earth and Planetary Science Letters 333-334, 226-237.

O'Driscoll, B., Derbyshire, E.J., Gertisser, R., 2012b. Snapshots of ancient oceanic mantle captured in British and Irish ophiolites. Geology Today, 28(4), 134-140.

O'Driscoll, B., Walker, R.J., Day, J.M.D., Ash, R.D., Daly, J.S. 2015. Generations of melt extraction, melt-rock interaction and high-temperature metasomatism preserved in peridotites of the ~497 Ma Leka Ophiolite Complex, Norway. Journal of Petrology, 56(9), 1797-1828.

O'Driscoll, B., González-Jiménez, J.M., 2016. Petrogenesis of the platinum-group minerals. Reviews in Mineralogy and Geochemistry, Mineralogical Society of America, Volume 81, 489-578.

Park, J-W., Kamenetsky, V., Campbell, I., Park, G., Hanski, E., Pushkarev, E. 2017. Empirical constraints on partitioning of platinum group elements between Cr-spinel and primitive terrestrial magmas. Geochimica et Cosmochimica Acta, 216, 393-416.

Oliver, G. J. H., McAlpine, R. R., 1998. Occurrence of a sheeted dyke complex in the Ballantrae ophiolite, Scotland. Geological Magazine 135, 509-517.

Oliver, G. J. H., Stone, P., Bluck, B. J., 2002. The Ballantrae Complex and Southern Uplands terrane, in: Trewin, N. H. (Ed.), The Geology of Scotland (2nd Edition). The Geological Society, London, pp. 167-200.

Orberger, B., Lorand, J-P., Girardeau, J., Mercier, J. C. C., Pitragool, S., 1995. Petrogenesis of ultramafic rocks and associated chromitites in the Nan Uttaradit ophiolite, northern Thailand. Lithos 35, 153-182.

Pagé, P., Barnes, S-J., 2009. Using Trace Elements in Chromites to Constrain the Origin of Podiform Chromitites in the Thetford Mines Ophiolite, Québec, Canada. Economic Geology 104, 997-1018.

Peach, B. M., Horne, J., 1899. The Silurian rocks of Great Britain. Volume I, Scotland. Memoir of the Geological Survey of Great Britain 18, pp. 1-749.

Piccardo, G. B., Zanetti, A., Muntener, O., 2007. Melt/peridotite interaction in the Southern Lanzo peridotite: Field, textural and geochemical evidence. Lithos 94, 181-209.

Pleše, P., Higgins, M.D., Baker, D.R., Lanzafame, G., Kudrna Prašek, M., Mancini, L., Rooyakkers, S.M., 2019. Production and detachment of oxide crystal shells on bubble walls during experimental vesiculation of andesitic magmas. Contributions to Mineralogy and Petrology 174, 21.

Power, M., Pirrie, D., 2004. Platinum-group minerals within the Ballantrae Complex, SW Scotland. Scottish Journal of Geology 40, 1-5.

Prichard, H. M., Lord, R. A., Neary, C. R., 1996. A model to explain the occurrence of Platinum- and Palladium-rich ophiolite complexes. Journal of the Geological Society 153, 323-328.

Prichard, HM., Barnes, SJ., Godel, B., Reddy, SM., Vukmanovic, Z., Halfpenny, A., Neary, CR., Fisher, PC., 2015. The structure and origin of nodular chromite from the Troodos ophiolite, Cyprus, revealed using high-resolution X-ray computed tomography and electron backscatter diffraction. Lithos 218-219, 87-98.

Prichard, HM., Barnes, SJ., Godel, B., 2018. A mechanism for chromite growth in ophiolite complexes: evidence from 3D high-resolution X-ray computed tomography images of chromite

grains in Harold's Grave chromitite in the Shetland ophiolite. Mineralogical Magazine 82(3), 457-470.

Princivalle, F., Della Giusta, A., Carbonin, S., 1989. Comparative crystal chemistry of spinels from some suites of ultramafic rocks. Mineralogy and Petrology 40, 117- 126.

Princivalle, F., Della Giusta, A., De Min, A., Piccirillo, E. M., 1999. Crystal chemistry and significance of cation ordering in Mg-Al rich spinels from high-grade hornfels (Predazzo-Monzoni, NE Italy). Mineralogical Magazine 63, 257-262.

Pringle, J., 1935. British Regional Geology: the south of Scotland. HMSO, Edinburgh.

Rampone, E., Piccardo, G. B., Hofmann, A.W., 2008). Multi-stage melt-rock interaction in the Mt. Maggiore (Corsica, France) ophiolitic peridotites: microstructural and geochemical evidence. Contributions to Mineralogy and Petrology 156, 453-475.

Rollinson, H., 2005. Chromite in the mantle section of the Oman ophiolite: a genetic model. The Island Arc 14, 542-550.

Rollinson, H., 2008. The geochemistry of mantle chromites from the northern part of the Oman ophiolite: inferred parental melt compositions. Contributions to Mineral Petrology 156, 273-288.

Rollinson, H., Adetunji, J., 2013. Mantle podiform chromitites do not form beneath midocean ridges: a case study from the Moho transition zone of the Oman ophiolite. Lithos 177, 314-327.

Ryan, P. D., Dewey, J. F., 1991. A geological and tectonic cross-section of the Caledonides of western Ireland. Journal of the Geological Society 148, 173-180.

Sack, R. O., Ghiroso, M. S., 1991. Chromium spinels as petrogenetic indicators: thermodynamics and petrological applications. American Mineralogist 76, 827-847.

Sheldrick, G. M., 1997. SHELX-97 Program for crystal structure refinement. University of Göttingen, Germany.

Smellie, J. L., Stone, P., 1992. Geochemical control on the evolutionary history of the Ballantrae Complex, SW Scotland, from comparisons with recent analogues, in: Parson, L. M., Murton, B.J., Browning, P. (Eds.), Ophiolites and their Modern Analogues. Geological Society of London, Special Publications 60, 171-178.

Smellie, J. L., Stone, P., 2001. Geochemical characteristics and geotectonic setting of early Ordovician basalt lavas in the Ballantrae Complex ophiolite, SW Scotland. Transactions of the Royal Society of Edinburgh: Earth Sciences 91, 539-555.

Smellie, J. L., Stone, P., Evans, J., 1995. Petrogenesis of boninites in the Ordovician Ballantrae Complex ophiolite, southwestern Scotland. Journal of Volcanology and Geothermal Research 69, 323-342.

Stone, P., Smellie, J. L., 1988. *The Ballantrae area: a description of the solid geology of parts of 1:25 000 sheets NX08, 18 and 19*. Classical areas of British Geology. HMSO for British Geological Survey.

Stone, P., 2014. A review of geological origins and relationships in the Ballantrae Complex, SW Scotland. Scottish Journal of Geology 50(1), 1-25.

Strachan, R. A., Smith, M., Harris, A. L., Fettes, D. J., 2002. The Northern Highland and Grampian terranes, in: Trewin, N. H. (Ed.), The Geology of Scotland. The Geological Society, London, pp. 167-200.

Thirlwall, M. F., Bluck, B. J., 1984. Sr-Nd isotope and chemical evidence that the Ballantrae 'ophiolite', SW Scotland, is polygenetic, in: Gass, I. G., Lippard, S. J., Shelton, A. W. (Eds.), Ophiolites and Oceanic Lithosphere, Geological Society of London Special Publications 13, 215-230.

Uchida, H., Lavina, B., Downs, R. T., Chesley, J., 2005. Single-crystal X-ray diffraction of spinels from the San Carlos Volcanic Field, Arizona: spinel as a geothermometer. American Mineralogist 90, 1900-1908.

Uysal, I., Tarkian, M., Burhan Sadilar, M., Zaccarini, F., Meisel, T., Garuti, G., Heidrich, S., 2009. Petrology of Al- and Cr-rich ophiolitic chromitites from the Mugla, SW Turkey: implications from composition of chromite, solid inclusions of platinum group mineral, silicate, and base-metal Contributions to Mineralogy and Petrology 158, 659-674.

Voigt, M., von der Handt, A., 2011. Influence of subsolidus processes on the chromium number in spinel in ultramafic rocks. Contributions to Mineralogy and Petrology 162, 675-689.

Vuollo, J., Liipo, J., Nykänen, V., Piirainnen, T., Pekkarinen, L., Tuokko, I., Ekdahl, E., 1995. An early Proterozoic podiform chromitite in the Outokumpu Ophiolite Complex, Finland. Economic Geology 90, 445-452.

Whattam, S. A., Stern, R. J., 2011. The 'subduction initiation rule': a key for linking ophiolites, intra-oceanic forearcs, and subduction initiation. Contributions to Mineralogy and Petrology 162, 1031-1045.

Wilkinson, J. M., Cann, J. R., 1974. Trace elements and tectonic relationships of basaltic rocks in the Ballantrae igneous complex, Ayrshire. Geological Magazine 111, 35- 41.

Xiong, F., Yang, J., Robinson, P.T., Xu, X., Liu, Z., Zhou, W., Feng, G., Xu, J., Li, J. and Niu, X. 2017. High-Al and high-Cr podiform chromitites from the western Yarlung-Zangbo suture zone, Tibet: Implications from mineralogy and geochemistry of chromian spinel, and platinum-group elements. Ore Geology Reviews 80, 1020-1041.

Zagrtdenov, NR, Ceuleneer, G., Rospabé, M., Borisova, AY., Toplis, MJ., Benoit, M. and Abily, B. 2018. Anatomy of a chromitite dyke in the mantle/crust transition zone of the Oman ophiolite. Lithos 312-313, 343-357.

Zhou, M-F., Robinson, P. T., 1997. Origin and tectonic environment of podiform chromite deposits. Economic Geology 92, 259-262.

Zhou, M-F., Robinson, P. T., Malpas, J., Li, Z., 1996. Podiform chromites in the Luobusa Ophiolite (Southern Tibet): Implications for melt-rock interaction and chromite segregation in the upper mantle. Journal of Petrology 37, 3-21.

Zhou, M-F., Malpas, J., Robinson, P. T., Sun, M., Li, J-W., 2001. Crystallisation of podiform chromitites from silicate magmas and the formation of nodular textures. Resource Geology 51, 1-6.

Figure Captions

Figure 1. Geological sketch map of the Ballantrae Ophiolite Complex, Scotland, showing the major lithological units and the locations of the Pinbain Bridge and Poundland Burn chromitite bodies. The sketch map is adapted from those in Stone (2014). The inset is a regional map of Scotland showing the regional location of the BOC in Ayrshire (red square).

Figure 2. (a) Field photograph illustrating typical harzburgite texture at Pinbain Bridge. (b) Nodular chromitite at Poundland Burn; the nodules are up to 1 cm in diameter and are hosted in a serpentinised dunite matrix. (c) Anti-nodular chromitite in close proximity to (b). The silicate nodules comprise serpentinite and are <1 cm in size, with a groundmass network of fine-grained Cr-spinel crystals. Pen-tip is shown for scale in (a) – (c).

Figure 3. (a-b) Backscattered electron micrographs of chromitite textures from Pinbain Bridge. Note the thin discontinuous Fe-rich (bright) rim on the grey Cr-spinel crystal in (a) and the fracture and associated brittle deformation in chromitite in (b). In (a) and (b), the black-coloured groundmass is predominantly serpentinite. (c) Thin section scan of BA-10-06 nodular-textured chromitite. The cuspate-shaped areas infilled with silicate in nodule centres (located within the red outline in one nodule) and relatively massive outer nodule mantles are described in the text. (d) Plane polarised light photomicrograph of orthopyroxene pseudomorph in a serpentinised harzburgite from Poundland Burn, in which bastite is partly replacing orthopyroxene. (e) Plane polarised light photomicrograph of Poundland Burn dunite – note the elongate stringer of Cr-spinel crystals (black) in the bottom-right of the image, as well as other isolated Cr-spinel crystals elsewhere in the serpentinised olivine groundmass. (f) Backscattered electron micrograph of accessory Cr-spinel from Poundland Burn dunite, with relatively thick Fe-rich rim and abundant silicate inclusions. The white arrows highlight stepped edges at the margins of the Cr-spinel crystal.

Figure 4. Panels illustrate the internal structure and chemical composition of a single Cr-spinel nodule from Poundland Burn (Sample BA-10-06). (a) Thin section scan showing the location (red square) of the nodule featured in (b) and (c). (b) Mineral chemical transect of the nodule, showing the relative homogeneity in Mg#, Cr# and TiO_2 from one side to the other. The transect represents 40 individual spot points, from X-Y, taken at equal spacings apart on the traverse shown in (c), but avoiding inclusions and fractures. (c) Stitched backscattered electron micrographs, showing the internal structure of an individual nodule and the position of the electron microprobe traverse shown in (b). The white arrows highlight stepped edges at the margins of the Cr-spinel nodule.

Figure 5. Plots of (a) Cr# versus Mg# and (b) TiO_2 versus Cr# discriminate the tectonic setting (and parental melt composition) of the Ballantrae Cr-spinels. In (a), the two solid black outline ellipses delineate the range of Pinbain Bridge and Poundland Burn chromitite compositions. The fields for boninite and abyssal peridotite are taken from Dick and Bullen (1984) and Kepezhinskas et al. (1993). The green field is the range of peridotite accessory Cr-spinel compositions referred to in Dare et al. (2009); it is important to note that the Ballantrae chromitite Cr-spinels fall outside of the outer limits of this field. In (b), the fields for MORB/boninite and layered intrusions, ophiolites and komatiites, come from Hunt et al. (2012) and references therein.

Figure 6. Trace element characteristics of the Ballantrae Cr-spinels. (a) V versus Cr#, (b) Co versus Cr#, (c) Ga versus Cr# and (d) Cu/Zn versus Cu/Ni. The symbols are the same as in **Figure 5**. Ranges of trace element compositions for the Lizard, Shetland and Corrycharmaig are shown for comparison (B O'Driscoll; unpublished data). The MORB and two boninite compositions come from Pagé and Barnes (2009). The Troodos arc picrite data are from Park et al. (2017). The symbols are the same as for **Figure 5**, unless otherwise specified.

Figure 7. Spidergram showing the major and trace element characteristics of the Ballantrae Cr-spinels, relative to two boninite compositions, and normalised to MORB. The boninite and MORB compositions are taken from Pagé and Barnes (2009). Abbreviations as follows: TMO, Thetford Mines Ophiolite; EPR, East Pacific Rise. See text for further discussion.

Figure 8. (a) Crystal structural analysis plot displaying cell edge length (a_0) against oxygen positional parameter (u). The majority of the Ballantrae Cr-spinels have low a_0 and higher u values

than the Shetland Ophiolite Complex Cr-spinels (orange field) from Derbyshire et al. (2013). (b) Cr-spinel crystal structural plot displaying Cr# versus oxygen positional parameter (*u*). The Pinbain Bridge Cr-spinels have higher Cr contents and correspondingly smaller *u* values whilst the Poundland Burn Cr-spinels display relatively consistent Cr contents across a small range in *u* (0.2629-0.2634). The symbols are the same as for **Figure 5**, unless otherwise specified.

Figure 9. (a) The Ti/Fe^3# versus Ga/Fe^3# diagram of Dare et al. (2009), illustrating that the Ballantrae Cr-spinels, in particular those from the Poundland Burn dunites, have compositions spanning the boundary between MOR-reacted and SSZ-reacted compositions (though mainly in the latter). The 'reacted' compositions refer to crystallisation by melt-rock reaction, in either a MOR or SSZ setting, whereas the residual field reflects accessory peridotite Cr-spinels unaffected by such processes. Chromitite compositions are plotted too for reference but these are probably unreliable for the reasons outlined in Dare et al. (2009). The ranges of compositions of Shetland, Lizard and Corrycharmaig Cr-spinels are also shown for comparison, and it is notable that the Lizard Cr-spinels in particular, which are an accessory phase in dunite, plot in the MOR-reacted field, consistent with published interpretations of the Lizard as a MORB-type ophiolite (O'Driscoll et al. 2012b). (b) Calculated TiO_2 versus Al_2O_3 for the Ballantrae Cr-spinel parental melts. See text for further discussion. The values for MORB and boninite, as well as the various boninite fields, come from Pagé and Barnes (2009). The grey-shaded boninite and MORB fields come from Rollinson (2008). The symbols are the same as for **Figure 5**, unless otherwise specified.

Sample	BA-10-03	BA-10-04	BA-10-06	BA-10-07	BA-10-10	BA-10-11	BA-10-12	BA-10-13
a_0	8.27043 (9)	8.2740 (4)	8.2206 (3)	8.2204 (3)	8.2205 (1)	8.2456 (4)	8.2528 (3)	8.2285 (5)

u	0.2625 (1)	0.2627 (1)	0.2630 (1)	0.2630 (1)	0.2631 (1)	0.2631 (1)	0.2629 (1)	0.2634 (2)
MgO	14.5 (2)	15.2 (2)	16.8 (3)	16.8 (3)	16.7 (2)	13.5 (3)	13.3 (2)	15.6 (3)
Al_2O_3	18.3 (2)	19.9 (4)	30.9 (4)	30.9 (2)	30.7 (4)	27.0 (5)	26.3 (5)	29.0 (1)
TiO_2	0.12 (2)	0.11 (1)	0.26 (1)	0.24 (2)	0.28 (2)	0.25 (2)	0.26 (2)	0.24 (2)
Cr_2O_3	50.4 (2)	49.3 (3)	37.4 (3)	37.5 (4)	37.6 (3)	34.3 (4)	33.7 (6)	36.8 (5)
MnO	0.21 (3)	0.21 (4)	0.18 (3)	0.18 (3)	0.19 (3)	0.25 (2)	0.24 (3)	0.19 (3)
FeO_{tot}	16.1 (2)	14.8 (1)	14.0 (2)	13.9 (2)	14.2 (1)	23.5 (7)	25.1 (4)	17.4 (2)
NiO	0.10 (3)	0.17 (4)	0.20 (1)	0.18 (4)	0.18 (4)	0.20 (3)	0.24 (2)	0.18 (3)
ZnO*	0.07 (2)		0.07 (2)		0.05 (2)	0.14 (3)	0.17 (3)	
Sum	99.84	99.74	99.84	99.65	99.88	99.25	99.27	99.41
FeO	12.6 (2)	11.6 (1)	11.0 (2)	11.1 (2)	11.3 (1)	15.2 (7)	15.4 (4)	12.6 (2)
Fe_2O_3	3.96	3.61	3.33	3.13	3.21	9.25	10.8	5.36
Sum	100.24	100.10	100.17	99.96	100.20	100.18	100.35	99.95
T site								
Mg	0.639 (7)	0.672 (8)	0.683 (9)	0.66 (1)	0.663 (8)	0.55 (1)	0.540 (9)	0.639 (9)
Al	0.027 (1)	0.026 (2)	0.029 (2)	0.042 (2)	0.028 (2)	0.025 (2)	0.032 (2)	0.015 (1)
Mn	0.006 (1)	0.006 (1)	0.004 (1)	0.004 (1)	0.005 (1)	0.006 (1)	0.006 (1)	0.005 (1)
Fe^{2+}	0.295 (4)	0.297 (4)	0.242 (4)	0.263 (5)	0.267 (4)	0.38 (1)	0.379 (9)	0.311 (5)
Fe^{3+}	0.032 (4)		0.040 (6)	0.034 (7)	0.036 (5)	0.040 (7)	0.040 (4)	0.030 (4)
Zn	0.002 (1)		0.002 (1)		0.001 (1)	0.003 (1)	0.004 (1)	
M site								
Mg	0.028 (2)	0.027 (2)	0.044 (2)	0.070 (4)	0.058 (2)	0.057 (4)	0.059 (3)	0.042 (2)
Al	0.643 (6)	0.68 (1)	1.03 (1)	1.020 (8)	1.030 (9)	0.94 (1)	0.91 (1)	0.998 (7)
Ti	0.003 (1)	0.003 (1)	0.006 (1)	0.005 (1)	0.006 (1)	0.006 (1)	0.006 (1)	0.005 (1)
Cr	1.234 (6)	1.195 (9)	0.858 (8)	0.862 (9)	0.861 (7)	0.81 (1)	0.81 (1)	0.861 (9)
Fe^{2+}	0.028 (1)	0.002 (1)	0.024 (1)	0.006 (1)	0.007 (1)	0.007 (2)	0.013 (2)	
Fe^{3+}	0.061 (5)	0.086 (8)	0.031 (6)	0.033 (7)	0.034 (5)	0.17 (1)	0.20 (1)	0.089 (7)
Ni	0.003 (1)	0.004 (1)	0.005 (1)	0.004 (1)	0.004 (1)	0.005 (1)	0.006 (1)	0.004 (1)
F(X)	0.23	0.27	0.09	0.05	0.14	0.21	0.05	0.20
T°C	853	793	623	708	630	724	789	591

Table 1. Cell parameters, chemical analyses and cation distribution of Cr-spinels analysed by X-ray single crystal diffraction. Mean chemical analyses (up to 15 spot analyses for each crystal) and cation distribution in T and M site of the analyzed Cr-spinels on the basis of four oxygen atoms per formula unit. Fe^{3+} from stoichiometry. a_0: cell parameter (Å); *u*: oxygen positional parameter;. F(x): minimization factor, which takes into account the mean of square differences between calculated and observed parameters, divided by their standard deviations. Estimated standard deviations are in brackets. Intracrystalline closure temperature calculated by using the Princivalle et al. (1999) thermometer. *Zinc distribution is not reported when the standard deviation on chemistry is higher than the half of the mean value.

Chromitite petrogenesis in the mantle section of the Ballantrae Ophiolite Complex (Scotland)

Derbyshire, EJ[1], O'Driscoll, B[2*], Lenaz, D[3], Zanetti, A[4] and Gertisser, R[1]

[1]School of Geography, Geology and the Environment, Keele University, Keele, ST5 5BG, UK
[2]School of Earth and Environmental Sciences, University of Manchester, Oxford Road, M13 9PL, UK
[3]Dipartimento di Matematica e Geoscienze, Università degli Studi di Trieste, Trieste, I-34127, Italy
[4]Istituto di Geoscienze e Georisorse, C.N.R., Pavia, Italy

[*]Corresponding author: brian.odriscoll@manchester.ac.uk

Highlights:

- Chromitite in the Ballantrae ophiolite formed by channelized melt-rock reaction
- Significant compositional differences in chromitites from the Ballantrae ophiolite
- Calculated chromitite parental melts approximate both MORB-like and arc magmas
- Ballantrae chromitites formed during melt extraction in an evolving subduction zone